Block-Level MU-MISO Interference Exploitation Precoding: Optimal Structure and Explicit Duality

Junwen Yang, *Graduate Student Member, IEEE*, Ang Li, *Senior Member, IEEE*, Xuewen Liao, *Member, IEEE*, Christos Masouros, *Fellow, IEEE*, and A. Lee Swindlehurst, *Fellow, IEEE*

***Abstract*—This article investigates block-level interference exploitation (IE) precoding for multiuser multiple-input–single-output (MU-MISO) downlink systems. To overcome the need for symbol-level IE precoding to frequently update the precoding matrix, we propose to jointly optimize all the precoders or transmit signals within a transmission block. The resultant precoders only need to be updated once per block, and while not necessarily constant over all the symbol slots, we refer to the technique as block-level slot-variant IE precoding. Through a careful examination of the optimal structure and the explicit duality inherent in block-level power minimization (PM) and signal-to-interference-plus-noise ratio (SINR) balancing (SB) problems, we discover that the joint optimization can be decomposed into subproblems with smaller variable sizes. As a step further, we propose block-level slot-invariant IE precoding by adding a structural constraint on the slot-variant IE precoding to maintain a constant precoder throughout the block. A novel linear precoder for IE is further presented, and we prove that the proposed slot-variant and slot-invariant IE precoding share an identical solution when the number of symbol slots does not exceed the number of users. Numerical simulations demonstrate that the proposed precoders achieve a significant complexity reduction compared against benchmark schemes, without sacrificing performance.**

***Index Terms*—Block-level precoding, interference exploitation (IE), interference management, multiuser multiple-input–single-output (MU-MISO), power minimization (PM), signal-to-interference-plus-noise ratio (SINR) balancing (SB), symbol-level precoding (SLP).**

I. Introduction

With the ever-growing demand for high-data rates and massive access in wireless communications, independent data streams need to be spatially multiplexed in the same resource block via multiple-input–multiple-output (MIMO) or multiuser multiple-input–single-output (MU-MISO) systems [1], [2], [3]. Transmit precoding/beamforming is a predominant interference management technology for MIMO communications [4], [5]. Linear precoding methods leverage only the channel state information (CSI) to design the precoder, but ignore the actual information that is being transmitted. For example, zero forcing (ZF) [6] and regularized ZF (RZF) precoding [7] use (regularized) channel inversion to eliminate interference, but the inversion operation results in limited communication performance. On the other hand, nonlinear precoding methods have been proposed, such as dirty-paper precoding (DPC) [8], Tomlinson–Harashima precoding (THP) [5], and vector perturbation (VP) precoding [9], where the precoded signal is a nonlinear function of the data symbols. However, the complexity of the above nonlinear precoding methods limit their practical implementation [5], [8], [9].

To improve interference management, optimal linear precoding has been proposed, which models the precoding task as an optimization problem. A variety of optimization techniques have been investigated to seek solutions under different optimality criteria. Power minimization (PM) linear precoding can minimize the transmit power while guaranteeing given Quality-of-Service (QoS) conditions, which are commonly expressed in terms of signal-to-interference-plus-noise ratio (SINR) constraints [10], [11]. SINR balancing (SB) linear precoding aims to provide fairness among users by maximizing the minimum SINR of all the users in the system, usually subject to a transmit power constraint [12], [13].

The aforementioned interference management methods treat the interference as a harmful component that should be

Manuscript received 22 April 2024; revised 7 July 2024; accepted 26 July 2024. Date of publication 5 August 2024; date of current version 24 October 2024. The work of Ang Li was supported in part by the Young Elite Scientists Sponsorship Program by CIC under Grant 2021QNRC001; in part by the National Natural Science Foundation of China under Grant 62101422 and Grant 62371386; in part by the Science and Technology Program of Shaanxi Province under Grant 2024JC-JCQN-59; and in part by the Open Research Fund of the National Mobile Communications Research Laboratory, Southeast University, under Grant 2024D01. The work of Xuewen Liao was supported in part by the Shaanxi Science and Technology Innovation Team under Grant 2023-CX-TD-03; in part by the National Key Research and Development Program of China under Grant 2021YFB2900501; and in part by the Science and Technology Program of Shaanxi Province under Grant 2021GXLH-Z-038. The work of Christos Masouros was supported by the Project 6GMUSICAL part of the Smart Networks and Services Joint Undertaking (SNS JU) under the European Union's Horizon Europe Research and Innovation Programme with Grant under Agreement 101139176. The work of A. Lee Swindlehurst was supported by the U.S. National Science Foundation under Grant CCF-2008724. *(Corresponding authors: Xuewen Liao; Ang Li.)*

Junwen Yang is with the School of Information and Communications Engineering, Faculty of Electronic and Information Engineering, Xi'an Jiaotong University, Xi'an 710049, Shaanxi, China (e-mail: jwyang@stu.xjtu.edu.cn).

Ang Li is with the School of Information and Communications Engineering, Faculty of Electronic and Information Engineering, Xi'an Jiaotong University, Xi'an 710049, Shaanxi, China, and also with the National Mobile Communications Research Laboratory, Southeast University, Nanjing 210096, China (e-mail: ang.li.2020@xjtu.edu.cn).

Xuewen Liao is with the Shaanxi Key Laboratory of Deep Space Exploration Intelligent Information Technology, School of Information and Communications Engineering, Faculty of Electronic and Information Engineering, Xi'an Jiaotong University, Xi'an 710049, Shaanxi, China (e-mail: yeplos@mail.xjtu.edu.cn).

Christos Masouros is with the Department of Electronic and Electrical Engineering, University College London, WC1E 7JE London, U.K. (e-mail: c.masouros@ucl.ac.uk).

A. Lee Swindlehurst is with the Center for Pervasive Communications and Computing, University of California, Irvine, CA 92697 USA (e-mail: swindle@uci.edu).

Digital Object Identifier 10.1109/JIOT.2024.3438569

eliminated. However, recent studies on interference exploitation (IE) have provided the novel insight that the multiuser interference is beneficial when it is constructive, and can be exploited to improve detection performance. This technique is also referred to as constructive interference (CI) precoding [14], [15], [16], [17], [18], [19]. IE precoding is data symbol dependent, and the precoder is commonly updated on a symbol-by-symbol basis, so it is often referred to as symbol-level precoding (SLP) [17], [19], [20], [21], [22], [23], [24], [25]. Recently, the idea of IE via SLP has been studied in various emerging wireless communication fields, such as reconfigurable intelligent surface (RIS) [26], [27], [28], [29], low-resolution digital-to-analog converters (DACs) [30], [31], [32], and integrated sensing and communications (ISACs) [33], [34], [35].

As promising as symbol-level IE precoding is, its need to update the precoder in each symbol slot imposes implementation challenges that originate from the SLP design criteria. Based on this observation, a block-level transmit power constrained SB IE precoding algorithm was proposed in [36], where a constant IE precoder is designed for an entire transmission block/frame.

Given that the precoded symbol-level IE signal can be viewed as a nonlinear function of the data symbols on the block level, SLP is commonly classified as nonlinear precoding [37]. The CI-BLP proposed in [36] offers a potential linear method for IE precoding, since it designs a unified constant precoder for a collection of data symbols over a transmission block. However, the work of [36] primarily concentrates on the SB problem and specifically addresses the scenario where the number of symbol slots exceeds the number of users. It thus does not provide proofs for the generic existence of linear precoding for IE.

To further exploit the potential of block-level optimizations for IE, in this article we propose block-level slot-variant and slot-invariant IE precoding for both PM and SB problems. Here, "block-level" refers to the fact that the precoding optimization is solved once per block, while "slot-variant" indicates that the precoding solution can be considered as a time-varying linear transformation of the data symbols. The main contributions of this article are summarized below.

1) *Block-Level Slot-Variant IE Precoding:* We propose block-level PM and weighted SB slot-variant IE precoders using long-term performance metrics to reduce the precoder update frequency. In a single transmission block/frame, multiple precoders (or equivalently, transmit signals) are optimized with block-level performance metrics. The optimal structure of the precoders is derived for both PM and (weighted) SB problems to simplify their problem structure. We further prove that block-level PM slot-variant IE precoding and PM-SLP share the same optimal solution, and the relationship between SB slot-variant IE precoding and SB-SLP is also derived. The proposed relationship can be leveraged to decompose the slot-variant IE precoding problem into more tractable subproblems.
2) *Block-Level Slot-Invariant IE Precoding:* By introducing a structural constraint on the slot-variant IE precoding matrix, we obtain PM and weighted SB IE precoders that are invariant across the symbol slots within a transmission block/frame, and hence become block-level slot-invariant IE precoders. Their optimal structure is obtained by deriving the Lagrangian dual problems, while a novel explicit duality is revealed in the proof of the solutions to the two slot-invariant IE precoding problems. Thus, the more sophisticated weighted SB slot-invariant IE precoding problem can be solved through the simpler PM slot-invariant problem.
3) *Existence of Linear Precoding for IE:* On the premise that the number of symbol slots does not exceed the number of users, we prove the existence of a constant precoder over different symbol slots for arbitrary precoding, and reveal that the IE gain can be achieved by a linear precoder. This is contrary to the common assumption that IE precoders must be calculated in each symbol slot to fully exploit the multiuser interference. Under the aforementioned precondition, the proposed linear approach allows updating the precoder once per transmission block while fully preserving superior SLP performance, without compromising any SLP performance benefits.

Extensive numerical simulations are conducted to demonstrate the superiority of the proposed block-level slot-variant and slot-invariant IE precoding. The simulations also validate our derivations of the optimality of the linear precoder.

The remainder of this article is organized as follows. Section II introduces the system model and preliminaries. Section III presents the block-level PM/SB slot-variant IE precoding. Section IV investigates the block-level PM and weighted SB slot-invariant IE precoding. Section V proposes the novel linear precoder for IE. Section VI presents the numerical results, and Section VII concludes this article.

Notation: Scalars, vectors, and matrices are denoted by plain lower case, bold lower case, and bold capital letters, respectively. $(\cdot)^{\mathrm{T}}$, $(\cdot)^{H}$, and $(\cdot)^{-1}$ denote transpose, conjugate transpose, and inverse operators, respectively. $\mathbb{C}^{M\times N}$ and $\mathbb{R}^{M\times N}$ denote the sets of $M\times N$ matrices with complex and real entries, respectively. $|\cdot|$ represents the absolute value of a real scalar or the modulus of a complex scalar. $\|\cdot\|$ denotes the Euclidean norm of a vector or spectral norm of a matrix. $\|\cdot\|_F$ represents the Frobenius norm of a matrix. $\Re\{\cdot\}$ and $\Im\{\cdot\}$, respectively, denote the real part and imaginary part of a complex input. $\succeq$ denotes element-wise inequality. $\mathbf{0}$, $\mathbf{1}$, and $\mathbf{I}$ represent, respectively, the all-zeros vector, the all-ones vector, and the identity matrix. $\oslash$ denotes the element-wise division. $\mathrm{diag}\{\cdot\}$ returns a diagonal matrix with the entries of the input vector on the main diagonal.

II. System Model and Preliminaries

A. System Model

We consider a time-division duplex (TDD) MU-MISO downlink system with N_t transmit antennas and N_r single-antenna users. Assume the channel is constant over a transmission block/frame, which consists of N_s symbol slots.

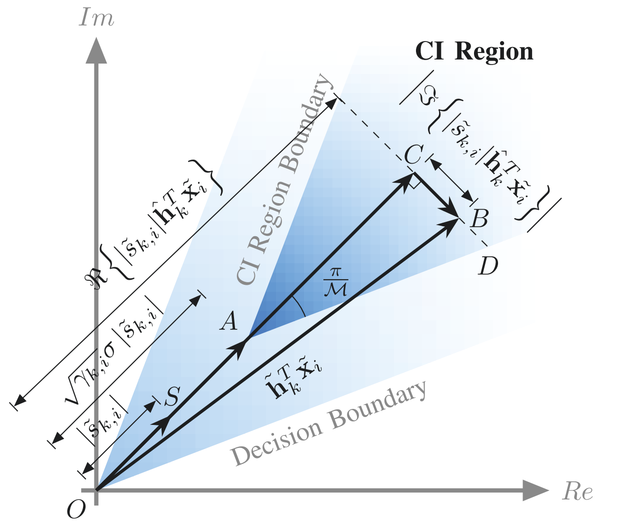

Fig. 1. Geometric interpretation of IE for a generic $\mathcal{M}$-PSK constellation.

The received signal $\tilde{y}_{k,i}$ at the kth user in the ith symbol slot can be represented as

$$\tilde{y}_{k,i} = \underbrace{\tilde{\mathbf{h}}_k^{\mathrm{T}} \tilde{\mathbf{w}}_i^k \tilde{s}_{k,i}}_{\text{desired signal}} + \underbrace{\sum_{g=1, g\neq k}^{N_r} \tilde{\mathbf{h}}_k^{\mathrm{T}} \tilde{\mathbf{w}}_i^g \tilde{s}_{g,i}}_{\text{interference}} + \underbrace{\tilde{z}_{k,i}}_{\text{noise}}$$
$$= \tilde{\mathbf{h}}_k^{\mathrm{T}} \tilde{\mathbf{W}}_i \tilde{\mathbf{s}}_{:,i} + \tilde{z}_{k,i} = \tilde{\mathbf{h}}_k^{\mathrm{T}} \tilde{\mathbf{x}}_i + \tilde{z}_{k,i} \quad (1)$$

where $\tilde{\mathbf{h}}_k \in \mathbb{C}^{N_t}$ represents the channel between the transmitter and the kth user; $\tilde{s}_{k,i}$ and $\tilde{z}_{k,i} \sim \mathcal{CN}(0, \sigma^2)$ denote the modulated data symbol and the additive white Gaussian noise of the kth user in the ith symbol slot; and $\tilde{\mathbf{W}}_i \triangleq [\tilde{\mathbf{w}}_i^1 \cdots \tilde{\mathbf{w}}_i^{N_r}] \in \mathbb{C}^{N_t \times N_r}$, $\tilde{\mathbf{s}}_{:,i} \triangleq [\tilde{s}_{k,i}, \ldots, \tilde{s}_{N_r,i}]^{\mathrm{T}}$, and $\tilde{\mathbf{x}}_i \triangleq \tilde{\mathbf{W}}_i \tilde{\mathbf{s}}_{:,i}$ denote the precoder, the data symbol vector, and the precoded transmit signal in the ith symbol slot, respectively. We assume phase-shift keying (PSK) signaling in this article, but the IE design can be readily extended to quadrature amplitude modulation (QAM) [36], [38]. The term "precoding technique" or "precoder design" refers to the computation of the precoder $\tilde{\mathbf{W}}_i$, and it can also mean the direct computation of the transmit signal vector $\tilde{\mathbf{x}}_i$. Given the transmit signal vector $\tilde{\mathbf{x}}_i$ and any data symbol vector $\tilde{\mathbf{s}}_{:,i}$, the precoder $\tilde{\mathbf{W}}_i$ can be obtained by the following expression [38]:

$$\tilde{\mathbf{W}}_i = \tilde{\mathbf{x}}_i \frac{\tilde{\mathbf{s}}_{:,i}^H}{\tilde{\mathbf{s}}_{:,i}^H \tilde{\mathbf{s}}_{:,i}}. \quad (2)$$

The precoding matrix varies with the symbol slots when slot-variant BLP or SLP is adopted. When slot-invariant BLP is employed at the transmitter, a constant precoding matrix will be used to precode all the $N_r \times N_s$ data symbols transmitted in one transmission block/frame. In such cases, we omit the subscript of the block-level slot-invariant precoder, i.e., $\tilde{\mathbf{W}}_i = \tilde{\mathbf{W}}_{j\neq i} = \tilde{\mathbf{W}}$.

B. Interference Exploitation

The interference term $\sum_{g=1,g\neq k}^{N_r} \tilde{\mathbf{h}}_k^{\mathrm{T}} \tilde{\mathbf{W}}_i \tilde{s}_{g,i}$ in (1) is often treated as noise to be eliminated or suppressed. On the contrary, with the aid of CSI and knowledge of the data symbols, IE precoding manages to convert the interference part of the received signal into CI by optimizing the noiseless received signal [18]. To measure the QoS of a specific IE precoding technique, we introduce the instantaneous SINR of the kth user in the ith symbol slot as $\mathrm{SINR}_{k,i} \triangleq (|\tilde{\mathbf{h}}_k^{\mathrm{T}} \tilde{\mathbf{x}}_i|^2/\sigma^2)$ [18], which can also be viewed as an indirect indicator of the degree of IE. Note that this definition differs from conventional SINR, as all interference is converted to CI through IE precoding, thus eliminating any interference term in the denominator.

It should be noted that the instantaneous SINR is effective only when the interference is exploited and the noiseless received signal is pushed into the detection region.[1] Fig. 1 gives a geometric interpretation of the idea of IE for a generic $\mathcal{M}$-PSK constellation, where $\overrightarrow{OS} = \tilde{s}_{k,i}$, $\overrightarrow{OA} = \sqrt{\gamma_{k,i}}\sigma \tilde{s}_{k,i}$, and $\overrightarrow{OB} = \tilde{\mathbf{h}}_k^{\mathrm{T}} \tilde{\mathbf{x}}_i$ denote the data symbol, the nominal received data symbol with instantaneous SINR threshold $\mathrm{SINR}_{k,i} = \gamma_{k,i} |\tilde{s}_{k,i}|^2$, and the noiseless received signal, respectively. We can observe that as long as the noiseless received signal $\overrightarrow{OB}$ lies in the CI region, IE is achieved with a certain SINR threshold. Leveraging the method proposed in [38], we orthogonally decompose $\overrightarrow{OB}$ along the direction of $\overrightarrow{OS}$, then we have $\overrightarrow{OB} = \overrightarrow{OC} + \overrightarrow{CB}$, where $\overrightarrow{CB}$ intersects with the nearest CI region boundary at point D. In this way, we can readily formulate the condition for the received signal to be located in the CI region as $|\overrightarrow{CD}| \geq |\overrightarrow{CB}|$. After some transformations, the CI constraints for the IE system can be written in terms of the instantaneous SINR threshold as [18]

$$\Re\left\{\hat{\mathbf{h}}_k^{\mathrm{T}} \tilde{\mathbf{x}}_i\right\} - \frac{\left|\Im\left\{\hat{\mathbf{h}}_k^{\mathrm{T}} \tilde{\mathbf{x}}_i\right\}\right|}{\tan \frac{\pi}{\mathcal{M}}} \geq \sqrt{\gamma_{k,i}}\sigma \quad \forall k \quad (3)$$

where $\hat{\mathbf{h}}_k^{\mathrm{T}} \triangleq (\tilde{\mathbf{h}}_k^{\mathrm{T}}/\tilde{s}_{k,i})$. Since the instantaneous SINR thresholds are incorporated into the CI constraints, we use the terms SINR constraints and CI constraints interchangeably in this article.

III. Block-Level Slot-Variant Interference-Exploitation Precoder

In this section, we propose a slot-variant IE precoder that only needs to compute the precoders or transmit signal vectors once per transmission block/frame while coherently considering the communication performance for all the symbol slots. Moreover, the proposed block-level optimizations can achieve long-term operation, instead of focusing only on the short-term symbol-level design metrics.

A. PM Slot-Variant IE Precoder

To design a slot-variant IE precoder for the PM problem, the transmitter aims to minimize the block-level transmit power while satisfying the prescribed SINR constraints for the noiseless received signal of all the N_r users over each symbol slot. Therefore, the symbol-level transmit power objective function in the PM-SLP problem mentioned in [18] is relaxed to the block-level transmit power. This allows for a joint

[1] We consider uncoded systems in this article, but IE precoding can also be applied to coded systems [39], [40].

optimization of the precoder over a collection of symbol slots within a transmission block. It can be formulated in each transmission block as

$$\begin{aligned}\min_{\{\tilde{\mathbf{x}}_i\}} \quad & \sum_{i=1}^{N_s} \left\|\tilde{\mathbf{x}}_i\right\|^2 \\ \text{s.t.} \quad & \Re\left\{\hat{\mathbf{h}}_k^{\mathrm{T}}\tilde{\mathbf{x}}_i\right\} - \frac{\left|\Im\left\{\hat{\mathbf{h}}_k^{\mathrm{T}}\tilde{\mathbf{x}}_i\right\}\right|}{\tan\frac{\pi}{\mathcal{M}}} \geq \sqrt{\gamma_{k,i}}\sigma \quad \forall k \quad \forall i. \end{aligned} \tag{4}$$

The formulation in (4) is a linearly constrained quadratic programming problem, and thus is convex. Although it can be solved using standard optimization tools like CVX, efficiently addressing it with customized algorithms poses challenges. The first and foremost obstacle is the complex-valued optimization variables and sophisticated constraint structure. Therefore, we reformulate problem (4) into a real-valued equivalent form with explicit linear constraints

$$\min_{\{\mathbf{x}_i\}} \sum_{i=1}^{N_s}\|\mathbf{x}_i\|^2 \text{ s.t. } \mathbf{T}\hat{\mathbf{S}}_i\mathbf{H}\mathbf{x}_i \succeq \mathbf{b}_i \quad \forall i \tag{5}$$

where

$$\mathbf{x}_i \triangleq \begin{bmatrix}\Re\left\{\tilde{\mathbf{x}}_i\right\}\\ \Im\left\{\tilde{\mathbf{x}}_i\right\}\end{bmatrix} \in \mathbb{R}^{2N_t} \quad \forall i \tag{6a}$$

$$\mathbf{T} \triangleq \begin{bmatrix}\mathbf{I} & -\frac{1}{\tan\frac{\pi}{\mathcal{M}}}\mathbf{I}\\ \frac{1}{\tan\frac{\pi}{\mathcal{M}}}\mathbf{I} & \mathbf{I}\end{bmatrix} \in \mathbb{R}^{2N_r\times 2N_r} \tag{6b}$$

$$\hat{\mathbf{S}}_i \triangleq \begin{bmatrix}\Re\left\{\tilde{\mathbf{S}}_i\right\} & -\Im\left\{\tilde{\mathbf{S}}_i\right\}\\ \Im\left\{\tilde{\mathbf{S}}_i\right\} & \Re\left\{\tilde{\mathbf{S}}_i\right\}\end{bmatrix} \in \mathbb{R}^{2N_r\times 2N_r} \quad \forall i \tag{6c}$$

$$\tilde{\mathbf{S}}_i \triangleq \operatorname{diag}\left\{\mathbf{1} \oslash \tilde{\mathbf{s}}_{:,i}\right\} \in \mathbb{R}^{N_r\times N_r} \quad \forall i \tag{6d}$$

$$\mathbf{H} \triangleq \begin{bmatrix}\Re\left\{\tilde{\mathbf{H}}\right\} & -\Im\left\{\tilde{\mathbf{H}}\right\}\\ \Im\left\{\tilde{\mathbf{H}}\right\} & \Re\left\{\tilde{\mathbf{H}}\right\}\end{bmatrix} \in \mathbb{R}^{2N_r\times 2N_t} \tag{6e}$$

$$\tilde{\mathbf{H}} \triangleq \left[\tilde{\mathbf{h}}_1 \cdots \tilde{\mathbf{h}}_{N_s}\right]^{\mathrm{T}} \in \mathbb{R}^{N_r\times N_t} \tag{6f}$$

$$\mathbf{b}_i \triangleq \left[\tilde{\mathbf{b}}_i^{\mathrm{T}}\ \tilde{\mathbf{b}}_i^{\mathrm{T}}\right]^{\mathrm{T}} \in \mathbb{R}^{2N_r} \quad \forall i \tag{6g}$$

$$\tilde{\mathbf{b}}_i \triangleq \left[\sqrt{\gamma_{1,i}}\sigma \cdots \sqrt{\gamma_{N_r,i}}\sigma\right]^{\mathrm{T}} \in \mathbb{R}^{N_r} \quad \forall i. \tag{6h}$$

The real-valued PM problem for the slot-variant IE precoder has a simplified structure compared with the complex-valued one. It is however still not trivial to obtain the optimal solution due to the irregular polyhedral feasible region in (5). Since its convexity guarantees that the duality gap is zero, we can derive the optimal solution structure of (5) by further formulating its dual problem and leveraging Lagrangian duality.

B. Optimal Structure for PM Slot-Variant IE Precoder

To derive the optimal precoder structure, we first write the Lagrangian function of (5)

$$\mathcal{L}(\{\mathbf{x}_i\}, \{\boldsymbol{\lambda}_i\}) \triangleq \sum_{i=1}^{N_s}\|\mathbf{x}_i\|^2 + \boldsymbol{\lambda}_i^{\mathrm{T}}\left(\mathbf{b}_i - \mathbf{T}\hat{\mathbf{S}}_i\mathbf{H}\mathbf{x}_i\right) \tag{7}$$

where $\boldsymbol{\lambda}_i$ is the Lagrangian dual variable associated with the CI constraints in the ith symbol slot. The Karush–Kuhn–Tucker (KKT) optimal conditions are given by

$$\mathbf{T}\hat{\mathbf{S}}_i\mathbf{H}\mathbf{x}_i \succeq \mathbf{b}_i \quad \forall i \tag{8}$$

$$\boldsymbol{\lambda}_i \succeq \mathbf{0} \quad \forall i \tag{9}$$

$$\boldsymbol{\lambda}_{i,k}\left(\mathbf{b}_i - \mathbf{T}\hat{\mathbf{S}}_i\mathbf{H}\mathbf{x}_i\right)_k = 0 \quad \forall k \quad \forall i \tag{10}$$

$$\frac{\partial\mathcal{L}(\{\mathbf{x}_i\}, \{\boldsymbol{\lambda}_i\})}{\partial\mathbf{x}_i} = \mathbf{0} \quad \forall i \tag{11}$$

where $\boldsymbol{\lambda}_{i,k}$ and $(\mathbf{b}_i - \mathbf{T}\hat{\mathbf{S}}_i\mathbf{H}\mathbf{x}_i)_k$ denote the kth entry of $\boldsymbol{\lambda}_i$ and $\mathbf{b}_i - \mathbf{T}\hat{\mathbf{S}}_i\mathbf{H}\mathbf{x}_i$, respectively. From (11) we have

$$2\mathbf{x}_i - \mathbf{H}^{\mathrm{T}}\mathbf{T}^{\mathrm{T}}\hat{\mathbf{S}}_i^{\mathrm{T}}\boldsymbol{\lambda}_i = \mathbf{0} \quad \forall i. \tag{12}$$

Therefore, the optimal solution to (5) is given by

$$\mathbf{x}_i = \frac{1}{2}\mathbf{H}^{\mathrm{T}}\mathbf{T}^{\mathrm{T}}\hat{\mathbf{S}}_i^{\mathrm{T}}\boldsymbol{\lambda}_i \quad \forall i. \tag{13}$$

The dual problem of (5) is to maximize the dual function, i.e., $g(\{\boldsymbol{\lambda}_i\}) \triangleq \min_{\{\mathbf{x}_i\}} \mathcal{L}(\{\mathbf{x}_i\}, \{\boldsymbol{\lambda}_i\})$, subject to nonnegative constraints. It can be written as

$$\max_{\{\boldsymbol{\lambda}_i\}}\min_{\{\mathbf{x}_i\}} \ \mathcal{L}(\{\mathbf{x}_i\}, \{\boldsymbol{\lambda}_i\}) \text{ s.t. } \boldsymbol{\lambda}_i \succeq \mathbf{0} \quad \forall i. \tag{14}$$

By substituting the optimal solution structure (13) into the above dual problem, we can reformulate it in the following form:

$$\begin{aligned}\min_{\{\boldsymbol{\lambda}_i\}} \quad & \sum_{i=1}^{N_s}\frac{1}{4}\boldsymbol{\lambda}_i^{\mathrm{T}}\hat{\mathbf{S}}_i\mathbf{T}\mathbf{H}\mathbf{H}^{\mathrm{T}}\mathbf{T}^{\mathrm{T}}\hat{\mathbf{S}}_i^{\mathrm{T}}\boldsymbol{\lambda}_i - \boldsymbol{\lambda}_i^{\mathrm{T}}\mathbf{b}_i \\ \text{s.t.} \quad & \boldsymbol{\lambda}_i \succeq \mathbf{0} \quad \forall i. \end{aligned} \tag{15}$$

This problem is considerably simpler than the original problem in (5), as the polyhedral constraints are simplified into nonnegative constraints. In algorithm design, projecting a candidate solution onto a feasible region defined by a nonnegative constraint can be easily done.

C. SB Slot-Variant IE Precoder

In designing a block-level slot-variant IE precoder for the SB problem, we aim to achieve fairness among all the users over a transmission block by balancing the instantaneous received SINR. It can be seen from Fig. 1 that the

$$\begin{aligned}\max_{\{\tilde{\mathbf{x}}_i\}}\min_{k,i}\arg\min \quad & \left\{\frac{1}{\sqrt{\gamma_{k,i}}\sigma}\left(\Re\left\{\hat{\mathbf{h}}_k^{\mathrm{T}}\tilde{\mathbf{x}}_i\right\} - \frac{\Im\left\{\hat{\mathbf{h}}_k^{\mathrm{T}}\tilde{\mathbf{x}}_i\right\}}{\tan\frac{\pi}{\mathcal{M}}}\right), \frac{1}{\sqrt{\gamma_{k,i}}\sigma}\left(\Re\left\{\hat{\mathbf{h}}_k^{\mathrm{T}}\tilde{\mathbf{x}}_i\right\} + \frac{\Im\left\{\hat{\mathbf{h}}_k^{\mathrm{T}}\tilde{\mathbf{x}}_i\right\}}{\tan\frac{\pi}{\mathcal{M}}}\right)\right\} \\ \text{s.t.} \quad & \sum_{i=1}^{N_s}\left\|\tilde{\mathbf{x}}_i\right\|^2 \leq \sum_{i=1}^{N_s} p_i \end{aligned} \tag{16}$$

aforementioned rationale can be interpreted as maximizing the minimum amplitude of $\overrightarrow{OA}$ over N_s symbol slots, which is formulated as an optimization problem on the precoding matrix in (16), shown at the bottom of the previous page.

Since handling such a max-min problem is difficult, we recast it as a maximization problem by introducing an auxiliary variable t. The new problem can be formulated as

$$\begin{aligned}&\max_{\{\tilde{\mathbf{x}}_i\},\,t} \quad t\\ &\text{s.t.} \quad \Re\left\{\hat{\mathbf{h}}_k^{\mathrm{T}}\tilde{\mathbf{x}}_i\right\} - \frac{\left|\Im\left\{\hat{\mathbf{h}}_k^{\mathrm{T}}\tilde{\mathbf{x}}_i\right\}\right|}{\tan\frac{\pi}{\mathcal{M}}} \geq t\sqrt{\gamma_{k,i}}\sigma \quad \forall k \quad \forall i\\ &\qquad \sum_{i=1}^{N_s}\left\|\tilde{\mathbf{x}}_i\right\|^2 \leq \sum_{i=1}^{N_s} p_i \end{aligned} \tag{17}$$

where p_i denotes the transmit power budget for the ith symbol slot and $\sum_{i=1}^{N_s} p_i$ denotes the block-level transmit power budget. With a slight abuse of notation, we will let $(1/\sqrt{\gamma_{k,i}})$ denote the square root of the weight applied to $\text{SINR}_{k,i}$ in the context of the weighted SB problem. Similar to our manipulations on the PM problem, we again reformulate the above problem into a real-valued form

$$\begin{aligned}&\min_{\{\mathbf{x}_i\},t} \quad -t\\ &\text{s.t.} \quad \mathbf{T}\hat{\mathbf{S}}_i\mathbf{H}\mathbf{x}_i \succeq t\mathbf{b}_i \quad \forall i, \quad \sum_{i=1}^{N_s}\|\mathbf{x}_i\|^2 \leq \sum_{i=1}^{N_s} p_i \end{aligned} \tag{18}$$

where the definitions follow those in (6). This is a quadratically constrained linear programming problem, and thus is convex.

Proposition 1: The block level transmit power constraint in (18) is active when optimality is achieved, i.e.,

$$\sum_{i=1}^{N_s}\|\mathbf{x}_i\|^2 = \sum_{i=1}^{N_s} p_i. \tag{19}$$

Proof: Assume the above proposition does not hold, then the optimal solution satisfies $\sum_{i=1}^{N_s}\|\mathbf{x}_i\|^2 < \sum_{i=1}^{N_s} p_i$. Then we can always find a feasible solution $\{\dot{\mathbf{x}}_i\} = \alpha\{\mathbf{x}_i\}, \alpha > 1$, such that $\mathbf{T}\hat{\mathbf{S}}_i\mathbf{H}\dot{\mathbf{x}}_i \succ \alpha t\mathbf{b}_i \quad \forall i$, which contradicts the optimality of t. ■

Building upon Proposition 1, we will proceed to derive the optimal solution structure and formulate the Lagrangian dual problem in the following section.

D. Optimal Structure for SB Slot-Variant IE Precoder

The Lagrangian function of (18) is defined by

$$\begin{aligned}\mathcal{L}(\{\mathbf{x}_i\},\{\boldsymbol{\lambda}_i\},\mu) \triangleq\ & -t + \sum_{i=1}^{N_s}\boldsymbol{\lambda}_i^{\mathrm{T}}\left(t\mathbf{b}_i - \mathbf{T}\hat{\mathbf{S}}_i\mathbf{H}\mathbf{x}_i\right)\\ & + \mu\left(\sum_{i=1}^{N_s}\|\mathbf{x}_i\|^2 - \sum_{i=1}^{N_s} p_i\right)\end{aligned} \tag{20}$$

where $\boldsymbol{\lambda}_i$ is the Lagrangian dual variable associated with the CI constraints in the ith symbol slot and μ is the Lagrangian dual variable associated with the block-level transmit power constraint.

To derive the Lagrangian dual problem, we write the KKT optimality conditions below

$$\mathbf{T}\hat{\mathbf{S}}_i\mathbf{H}\mathbf{x}_i \succeq t\mathbf{b}_i \quad \forall i \tag{21}$$

$$\sum_{i=1}^{N_s}\|\mathbf{x}_i\|^2 \leq \sum_{i=1}^{N_s} p_i \tag{22}$$

$$\boldsymbol{\lambda}_i \succeq \mathbf{0} \quad \forall i \tag{23}$$

$$\mu \geq 0 \tag{24}$$

$$\boldsymbol{\lambda}_{i,k}\left(t\mathbf{b}_i - \mathbf{T}\hat{\mathbf{S}}_i\mathbf{H}\mathbf{x}_i\right)_k = 0 \quad \forall k \quad \forall i \tag{25}$$

$$\mu\left(\sum_{i=1}^{N_s}\|\mathbf{x}_i\|^2 - \sum_{i=1}^{N_s} p_i\right) = 0 \tag{26}$$

$$\frac{\partial\mathcal{L}(\{\mathbf{x}_i\},\{\boldsymbol{\lambda}_i\},\mu)}{\partial\mathbf{x}_i} = \mathbf{0} \quad \forall i \tag{27}$$

$$\frac{\partial\mathcal{L}(\{\mathbf{x}_i\},\{\boldsymbol{\lambda}_i\},\mu)}{\partial t} = 0 \tag{28}$$

where $\boldsymbol{\lambda}_{i,k}$ and $(t\mathbf{b}_i - \mathbf{T}\hat{\mathbf{S}}_i\mathbf{H}\mathbf{x}_i)_k$ denote the kth entry of $\boldsymbol{\lambda}_i$ and $t\mathbf{1} - \mathbf{T}\hat{\mathbf{S}}_i\mathbf{H}\mathbf{x}_i$, respectively. From Proposition 1, we see that the block-level transmit power constraint cannot be ignored, therefore $\mu \neq 0$. Then based on the stationarity condition in (27), we can directly write the optimal solution structure for the block-level SB slot-variant IE precoder as

$$\mathbf{x}_i = \frac{1}{2\mu}\mathbf{H}^{\mathrm{T}}\hat{\mathbf{S}}_i^{\mathrm{T}}\mathbf{T}^{\mathrm{T}}\boldsymbol{\lambda}_i \quad \forall i. \tag{29}$$

We can subsequently write the dual function as

$$\begin{aligned}g(\{\boldsymbol{\lambda}_i\},\mu) &\triangleq \min_{\{\mathbf{x}_i\}} \mathcal{L}(\{\mathbf{x}_i\},t,\{\boldsymbol{\lambda}_i\},\mu)\\ &= -\frac{1}{4\mu}\sum_{i=1}^{N_s}\boldsymbol{\lambda}_i^{\mathrm{T}}\mathbf{T}\hat{\mathbf{S}}_i\mathbf{H}\mathbf{H}^{\mathrm{T}}\hat{\mathbf{S}}_i^{\mathrm{T}}\mathbf{T}^{\mathrm{T}}\boldsymbol{\lambda}_i - \mu\sum_{i=1}^{N_s} p_i.\end{aligned} \tag{30}$$

Substituting the optimal solution structure (29) into (19), we can write μ in terms of $\{\boldsymbol{\lambda}_i\}$ as

$$\mu = \sqrt{\frac{\sum_{i=1}^{N_s}\boldsymbol{\lambda}_i^{\mathrm{T}}\mathbf{T}\hat{\mathbf{S}}_i\mathbf{H}\mathbf{H}^{\mathrm{T}}\hat{\mathbf{S}}_i^{\mathrm{T}}\mathbf{T}^{\mathrm{T}}\boldsymbol{\lambda}_i}{4\sum_{i=1}^{N_s} p_i}}. \tag{31}$$

Therefore, the optimal solution structure for the block-level SB slot-variant IE precoder in (29) turns out to be

$$\mathbf{x}_i = \sqrt{\frac{\sum_{i=1}^{N_s} p_i}{\sum_{i=1}^{N_s}\boldsymbol{\lambda}_i^{\mathrm{T}}\mathbf{T}\hat{\mathbf{S}}_i\mathbf{H}\mathbf{H}^{\mathrm{T}}\hat{\mathbf{S}}_i^{\mathrm{T}}\mathbf{T}^{\mathrm{T}}\boldsymbol{\lambda}_i}}\mathbf{H}^{\mathrm{T}}\hat{\mathbf{S}}_i^{\mathrm{T}}\mathbf{T}^{\mathrm{T}}\boldsymbol{\lambda}_i \quad \forall i. \tag{32}$$

By substituting (31) into (30), the dual variable μ therein can be eliminated. Thus the dual function can be reformulated as

$$\begin{aligned}g(\{\boldsymbol{\lambda}_i\}) &\triangleq \min_{\{\mathbf{x}_i\}} \mathcal{L}(\{\mathbf{x}_i\},t,\{\boldsymbol{\lambda}_i\},\mu)\\ &= -\sqrt{\sum_{j=1}^{N_s} p_j\sum_{i=1}^{N_s}\boldsymbol{\lambda}_i^{\mathrm{T}}\mathbf{T}\hat{\mathbf{S}}_i\mathbf{H}\mathbf{H}^{\mathrm{T}}\hat{\mathbf{S}}_i^{\mathrm{T}}\mathbf{T}^{\mathrm{T}}\boldsymbol{\lambda}_i}.\end{aligned} \tag{33}$$

Since the square root function is monotonic, the dual problem of (18) can be expressed as

$$\min_{\{\boldsymbol{\lambda}_i\}} \quad \sum_{i=1}^{N_s} \boldsymbol{\lambda}_i^{\mathrm{T}} \mathbf{T}\hat{\mathbf{S}}_i \mathbf{H}\mathbf{H}^{\mathrm{T}} \hat{\mathbf{S}}_i^{\mathrm{T}} \mathbf{T}^{\mathrm{T}} \boldsymbol{\lambda}_i$$
$$\text{s.t.} \quad \boldsymbol{\lambda}_i \succeq \mathbf{0} \ \ \forall i, \ \ \sum_{i=1}^{N_s} \mathbf{b}_i^{\mathrm{T}} \boldsymbol{\lambda}_i - 1 = 0. \tag{34}$$

This is a linearly constrained quadratic programming problem, and thus is convex. Compared to its primal problem (18), which is constrained by polyhedral CI constraints and a quadratic power constraint, the structure of the above dual problem is simplified. The complex CI and power constraints are converted to nonnegative constraints and a linear constraint.

E. Relationship to Traditional PM/SB-SLP

In this section, we begin by proving that block-level PM slot-variant IE precoding and PM-SLP share an identical optimal solution, then present the explicit duality between the block-level PM and SB slot-variant IE precoders, based on which we investigate the connections between block-level SB slot-variant IE precoding and conventional SB-SLP in [18].

In the ith symbol slot, the PM-SLP approach designs the transmit signal $\tilde{\mathbf{x}}_i$ using [18]

$$\min_{\tilde{\mathbf{x}}_i} \quad \left\|\tilde{\mathbf{x}}_i\right\|^2$$
$$\text{s.t.} \quad \Re\left\{\hat{\mathbf{h}}_k^{\mathrm{T}} \tilde{\mathbf{x}}_i\right\} - \frac{\left|\Im\left\{\hat{\mathbf{h}}_k^{\mathrm{T}} \tilde{\mathbf{x}}_i\right\}\right|}{\tan\frac{\pi}{\mathcal{M}}} \geq \sqrt{\gamma_{k,i}}\sigma \quad \forall k. \tag{35}$$

We summarize the connections between the proposed block-level PM slot-variant IE precoder and the existing PM-SLP in the following theorem.

Theorem 1: The block-level PM slot-variant IE precoder (4) and the PM-SLP precoder (35) have identical optimal solutions and precoding matrices in each symbol slot.

Proof: Note that in (4), the constraints on $\tilde{\mathbf{x}}_i$ are independent of the choice of other $\tilde{\mathbf{x}}_j \ \ \forall j \neq i$, and the contributions of each $\tilde{\mathbf{x}}_i$ to the criterion function do not depend on the other $\tilde{\mathbf{x}}_j \ \ \forall j \neq i$. Therefore, we can decompose the block-level PM slot-variant IE precoding problem (4) into N_s subproblems over the symbol slots and solve them independently, which means that the optimal solutions to the block-level PM slot-variant IE precoder and PM-SLP problems are identical. ■

The weighted SB-SLP problem in the ith symbol slot can be formulated as [18] and [38]

$$\max_{\tilde{\mathbf{x}}_i, t_i} \quad t_i$$
$$\text{s.t.} \quad \Re\left\{\hat{\mathbf{h}}_k^{\mathrm{T}} \tilde{\mathbf{x}}_i\right\} - \frac{\left|\Im\left\{\hat{\mathbf{h}}_k^{\mathrm{T}} \tilde{\mathbf{x}}_i\right\}\right|}{\tan\frac{\pi}{\mathcal{M}}} \geq t_i\sqrt{\gamma_{k,i}}\sigma \quad \forall k$$
$$\left\|\tilde{\mathbf{x}}_i\right\|^2 \leq p_i. \tag{36}$$

Before investigating the block-level SB slot-variant IE precoder's relationship to SB-SLP, let us review the explicit duality for PM/SB-SLP.

Lemma 1 (Duality for Symbol-Level IE Precoding [38]): The PM-SLP problem (35) and the SB-SLP problem (36) are dual problems. Let $\mathbf{x}_i^{PM}(\{\gamma_{k,i}\})$ and $p_i^{PM}(\{\gamma_{k,i}\}) \triangleq \|\mathbf{x}_i^{PM}(\{\gamma_{k,i}\})\|^2$ denote the optimal solution and the optimal value of the PM-SLP criterion (35) given $\{\gamma_{k,i}\}$, respectively. Then the counterparts for the SB-SLP problem (36), $\mathbf{x}_i^{SB}(\{\gamma_{k,i}\}, p_i)$ and $\mu_i^{SB}(\{\gamma_{k,i}\}, p_i)$, are given by

$$\tilde{\mathbf{x}}_i^{SB}\left(\left\{\gamma_{k,i}\right\}, p_i\right) = \sqrt{\frac{p_i}{p_i^{PM}\left(\left\{\gamma_{k,i}\right\}\right)}} \tilde{\mathbf{x}}_i^{PM}\left(\left\{\gamma_{k,i}\right\}\right) \tag{37}$$
$$t_i^{SB}\left(\left\{\gamma_{k,i}\right\}, p_i\right) = \sqrt{\frac{p_i}{p_i^{PM}\left(\left\{\gamma_{k,i}\right\}\right)}} \tag{38}$$

and vice versa as

$$\tilde{\mathbf{x}}_i^{PM}\left(\left\{\gamma_{k,i}\right\}\right) = \frac{1}{t_i^{SB}\left(\left\{\gamma_{k,i}\right\}, p_i\right)} \tilde{\mathbf{x}}_i^{SB}\left(\left\{\gamma_{k,i}\right\}, p_i\right) \tag{39}$$
$$p_i^{PM}\left(\left\{\gamma_{k,i}\right\}\right) = \frac{p_i}{\left(t_i^{SB}\left(\left\{\gamma_{k,i}\right\}, p_i\right)\right)^2}. \tag{40}$$

Proof: A detailed proof can be found in [38]. ■

A useful explicit duality for the block-level slot-variant IE precoders can be subsequently demonstrated below.

Theorem 2 (Duality for Block-Level Slot-Variant IE Precoding): The block-level PM slot-variant IE precoder in (4) and the SB slot-variant IE precoder in (17) are dual problems. Let $\{\tilde{\mathbf{x}}_i^{PM}(\{\gamma_{k,i}\})\}$ and $\sum_{i=1}^{N_s} p_i^{PM}(\{\gamma_{k,i}\}) \triangleq \sum_{i=1}^{N_s} \|\tilde{\mathbf{x}}_i^{PM}(\{\gamma_{k,i}\})\|^2$ denote the optimal solution and the optimal value of the block-level PM slot-variant IE precoding criterion (4) given $\{\gamma_{k,i}\}$, respectively. Then the counterparts for the block-level SB slot-variant IE precoding problem (17), $\{\tilde{\mathbf{x}}_i^{SB}(\{\gamma_{k,i}\}, \sum_{i=1}^{N_s} p_i)\}$ and $t^{SB}(\{\gamma_{k,i}\}, \sum_{i=1}^{N_s} p_i)$, are determined as

$$\tilde{\mathbf{x}}_i^{SB}\left(\left\{\gamma_{k,i}\right\}, \sum_{i=1}^{N_s} p_i\right) = \sqrt{\frac{\sum_{i=1}^{N_s} p_i}{\sum_{i=1}^{N_s} p_i^{PM}\left(\left\{\gamma_{k,i}\right\}\right)}} \times \tilde{\mathbf{x}}_i^{PM}\left(\left\{\gamma_{k,i}\right\}\right) \quad \forall i \tag{41}$$
$$t^{SB}\left(\left\{\gamma_{k,i}\right\}, \sum_{i=1}^{N_s} p_i\right) = \sqrt{\frac{\sum_{i=1}^{N_s} p_i}{\sum_{i=1}^{N_s} p_i^{PM}\left(\left\{\gamma_{k,i}\right\}\right)}} \tag{42}$$

and vice versa as

$$\tilde{\mathbf{x}}_i^{PM}\left(\left\{\gamma_{k,i}\right\}\right) = \frac{1}{t^{SB}\left(\left\{\gamma_{k,i}\right\}, \sum_{i=1}^{N_s} p_i\right)} \times \tilde{\mathbf{x}}_i^{SB}\left(\left\{\gamma_{k,i}\right\}, \sum_{i=1}^{N_s} p_i\right) \quad \forall i \tag{43}$$
$$\sum_{i=1}^{N_s} p_i^{PM}\left(\left\{\gamma_{k,i}\right\}\right) = \frac{\sum_{i=1}^{N_s} p_i}{\left(t^{SB}\left(\left\{\gamma_{k,i}\right\}, \sum_{i=1}^{N_s} p_i\right)\right)^2}. \tag{44}$$

Proof: The proof is similar to that of Lemma 1 and is therefore omitted. ■

Theorem 3: The optimal solutions to the block-level SB slot-variant IE precoding problem (17) and the SB-SLP problem (36) are symbol-level scaled versions of each other. Let $\tilde{\mathbf{x}}_i^{\mathrm{BL}}$ and $\tilde{\mathbf{x}}_i^{\mathrm{SL}}$ be the solutions in the ith symbol slot to the block-level SB slot-variant IE precoding problem (17) and the SB-SLP problem (36), respectively. These solutions are related as follows:

$$\tilde{\mathbf{x}}_i^{\mathrm{BL}} = \frac{1}{t_i}\sqrt{\frac{\sum_{j=1}^{N_s} p_j}{\sum_{j=1}^{N_s} \frac{p_j}{t_j^2}}}\tilde{\mathbf{x}}_i^{\mathrm{SL}} \quad \forall i \tag{45}$$

$$\tilde{\mathbf{x}}_i^{\mathrm{SL}} = \sqrt{\frac{p_i}{\left\|\tilde{\mathbf{x}}_i^{\mathrm{BL}}\right\|^2}}\tilde{\mathbf{x}}_i^{\mathrm{BL}} \quad \forall i. \tag{46}$$

Proof: From Theorem 2, we see that the block-level SB slot-variant IE precoder in (17) is a scaled version of the block-level PM slot-variant IE precoder in (4). Together with Theorem 1, it follows that the block-level SB slot-variant IE precoder in (17) is a power scaled version of the optimal solution to the PM-SLP problem (35). From Lemma 1, we further conclude that the block-level SB slot-variant IE precoder in (17) is a symbol-level scaled version of the optimal solution to the SB-SLP problem (36), and vice versa. The rest of this proof addresses (45) and (46).

Based on Lemma 1, the optimal transmit power for the PM-SLP problem is $p_i^{PM} = p_i$, and the optimal auxiliary variable for the SB-SLP problem is $t_i^{SB} = 1$. Therefore, the minimum instantaneous received SINRs in each symbol slot $\{t_i^{SB}\}$ are identical and equal to 1 in this case.

Given an arbitrary block-level transmit power budget, the optimal solution to the block-level SB slot-variant IE precoding problem (17) can be derived from the optimal solution to the SB-SLP problem (36) by normalizing the minimum instantaneous received SINRs to the same level, i.e., multiplying by $(1/t_i)$, and subsequently rescaling the transmit power to satisfy the block-level transmit power constraint by multiplying by $\sqrt{(\sum_{j=1}^{N_s} p_j/[\sum_{j=1}^{N_s} (p_j/t_j^2)])}$. Conversely, the optimal solution to the SB-SLP problem (36) can be obtained by rescaling the block-level SB slot-variant IE precoder such that it satisfies the symbol-level transmit power constraint. ■

In realistic systems, PM slot-variant precoding can be implemented by solving its Lagrangian dual problem as given in (15). Furthermore, according to Theorem 1, it can also be implemented by solving N_s PM-SLP problems. The efficient implementation of SB slot-variant precoding is demonstrated by Theorem 3.

IV. Block-Level Slot-Invariant Interference-Exploitation Precoder

To find a further compromise between performance and complexity, we design block-level PM and SB slot-invariant IE precoders in this section.

A. PM Slot-Invariant IE Precoder

The goal of the PM slot-invariant IE precoder is to minimize the block-level transmit power while adhering to CI constraints. In comparison to the PM slot-variant IE precoder design, this approach involves shifting the optimization variable from slot-variant IE precoders to a unified slot-invariant IE precoder. The optimization problem for the PM slot-invariant IE precoder is given by

$$\begin{aligned} \min_{\tilde{\mathbf{W}}} \quad & \sum_{i=1}^{N_s}\left\|\tilde{\mathbf{W}}\tilde{\mathbf{s}}_{:,i}\right\|^2 \\ \text{s.t.} \quad & \Re\left\{\hat{\mathbf{h}}_k^{\mathrm{T}}\tilde{\mathbf{W}}\tilde{\mathbf{s}}_{:,i}\right\} - \frac{\left|\Im\left\{\hat{\mathbf{h}}_k^{\mathrm{T}}\tilde{\mathbf{W}}\tilde{\mathbf{s}}_{:,i}\right\}\right|}{\tan\frac{\pi}{\mathcal{M}}} \geq \sqrt{\gamma_{k,i}}\sigma \quad \forall k \quad \forall i. \end{aligned} \tag{47}$$

This problem is a linearly constrained quadratic programming problem, and thus can be solved by off-the-shelf convex optimizers.

To rewrite the complex-valued problem in (47), we introduce the following set of real-valued matrices:

$$\mathbf{W} \triangleq \begin{bmatrix} \Re\{\tilde{\mathbf{W}}\} & -\Im\{\tilde{\mathbf{W}}\} \\ \Im\{\tilde{\mathbf{W}}\} & \Re\{\tilde{\mathbf{W}}\} \end{bmatrix} \in \mathbb{R}^{2N_t\times 2N_r} \tag{48a}$$

$$\overline{\mathbf{W}} \triangleq \begin{bmatrix} \Re\{\tilde{\mathbf{W}}\} & -\Im\{\tilde{\mathbf{W}}\} \end{bmatrix} \in \mathbb{R}^{N_t\times 2N_r} \tag{48b}$$

$$\mathbf{P}_1 \triangleq \begin{bmatrix} \mathbf{I} \\ \mathbf{0} \end{bmatrix} \in \mathbb{R}^{2N_t\times N_t} \tag{48c}$$

$$\mathbf{P}_2 \triangleq \begin{bmatrix} \mathbf{0} \\ \mathbf{I} \end{bmatrix} \in \mathbb{R}^{2N_t\times N_t} \tag{48d}$$

$$\mathbf{P}_3 \triangleq \begin{bmatrix} \mathbf{0} & \mathbf{I} \\ -\mathbf{I} & \mathbf{0} \end{bmatrix} \in \mathbb{R}^{2N_r\times 2N_r}. \tag{48e}$$

It is easy to verify that

$$\mathbf{W} = \mathbf{P}_1\overline{\mathbf{W}} + \mathbf{P}_2\overline{\mathbf{W}}\mathbf{P}_3 \tag{49}$$

$$\mathbf{P}_1^{\mathrm{T}}\mathbf{P}_1 = \mathbf{P}_2^{\mathrm{T}}\mathbf{P}_2 = \mathbf{I} \tag{50}$$

$$\mathbf{P}_1^{\mathrm{T}}\mathbf{P}_2 = \mathbf{P}_2^{\mathrm{T}}\mathbf{P}_1 = \mathbf{0}. \tag{51}$$

We are now prepared to formulate the real-valued problem that corresponds to the PM slot-invariant IE precoding problem (47)

$$\begin{aligned} \min_{\mathbf{W},\overline{\mathbf{W}}} \quad & \sum_{i=1}^{N_s}\left\|\mathbf{W}\mathbf{s}_{:,i}\right\|^2 \\ \text{s.t.} \quad & \mathbf{T}\hat{\mathbf{S}}_i\mathbf{H}\mathbf{W}\mathbf{s}_{:,i} \succeq \mathbf{b}_i \quad \forall i \\ & \mathbf{W} = \mathbf{P}_1\overline{\mathbf{W}} + \mathbf{P}_2\overline{\mathbf{W}}\mathbf{P}_3. \end{aligned} \tag{52}$$

The matrix constraint $\mathbf{W} = \mathbf{P}_1\overline{\mathbf{W}} + \mathbf{P}_2\overline{\mathbf{W}}\mathbf{P}_3$ is introduced to ensure that the optimal real-valued precoder $\mathbf{W}$ arranges the real and imaginary parts of the complex-valued precoder $\tilde{\mathbf{W}}$ as defined in (48). This problem can be simplified by eliminating the variable matrix $\mathbf{W}$

$$\begin{aligned} \min_{\overline{\mathbf{W}}} \quad & \sum_{i=1}^{N_s}\left\|\left(\mathbf{P}_1\overline{\mathbf{W}} + \mathbf{P}_2\overline{\mathbf{W}}\mathbf{P}_3\right)\mathbf{s}_{:,i}\right\|^2 \\ \text{s.t.} \quad & \mathbf{T}\hat{\mathbf{S}}_i\mathbf{H}\left(\mathbf{P}_1\overline{\mathbf{W}} + \mathbf{P}_2\overline{\mathbf{W}}\mathbf{P}_3\right)\mathbf{s}_{:,i} \succeq \mathbf{b}_i \quad \forall i. \end{aligned} \tag{53}$$

It can be seen that (53) preserves the quadratic objective function and linear constraints of (47). However, directly handling this problem is complicated due to the high-dimensional optimization variable $\overline{\mathbf{W}}$ and the underlying matrix structure constraint. To address this, we will examine the problem from a Lagrangian dual perspective in the following subsections.

B. Optimal Structure for PM Slot-Invariant IE Precoder

To formulate the Lagrangian dual problem, we begin by writing the Lagrangian function associated with (53) as follows:

$$\mathcal{L}\left(\overline{\mathbf{W}}, \{\boldsymbol{\lambda}_i\}\right) \triangleq \sum_{i=1}^{N_s} \left\| \left(\mathbf{P}_1\overline{\mathbf{W}} + \mathbf{P}_2\overline{\mathbf{W}}\mathbf{P}_3\right)\mathbf{s}_{:,i} \right\|^2 + \boldsymbol{\lambda}_i^{\mathrm{T}}\left[\mathbf{b}_i - \mathbf{T}\hat{\mathbf{S}}_i\mathbf{H}\left(\mathbf{P}_1\overline{\mathbf{W}} + \mathbf{P}_2\overline{\mathbf{W}}\mathbf{P}_3\right)\mathbf{s}_{:,i}\right] \tag{54}$$

where $\boldsymbol{\lambda}_i$ is the nonnegative Lagrange dual variable vector or Lagrange multiplier associated with the CI constraints $\mathbf{T}\hat{\mathbf{S}}_i\mathbf{H}(\mathbf{P}_1\overline{\mathbf{W}} + \mathbf{P}_2\overline{\mathbf{W}}\mathbf{P}_3)\mathbf{s}_{:,i} \succeq \mathbf{b}_i$ in the ith symbol slot. From the convexity of (53), the duality gap is zero. When the primal variable $\overline{\mathbf{W}}$ and dual variable $\{\boldsymbol{\lambda}_i\}$ achieve optimality, the following KKT conditions must be satisfied:

$$\mathbf{T}\hat{\mathbf{S}}_i\mathbf{H}\left(\mathbf{P}_1\overline{\mathbf{W}} + \mathbf{P}_2\overline{\mathbf{W}}\mathbf{P}_3\right)\mathbf{s}_{:,i} \succeq \mathbf{b}_i \quad \forall i \tag{55}$$

$$\boldsymbol{\lambda}_i \succeq \mathbf{0} \quad \forall i \tag{56}$$

$$\boldsymbol{\lambda}_{i,k}\left[\mathbf{T}\hat{\mathbf{S}}_i\mathbf{H}\left(\mathbf{P}_1\overline{\mathbf{W}} + \mathbf{P}_2\overline{\mathbf{W}}\mathbf{P}_3\right)\right]_{k,:}\mathbf{s}_{:,i} = \boldsymbol{\lambda}_{i,k}\mathbf{b}_{i,k} \quad \forall k \quad \forall i \tag{57}$$

$$\frac{\partial \mathcal{L}\left(\overline{\mathbf{W}}, \{\boldsymbol{\lambda}_i\}\right)}{\partial \overline{\mathbf{W}}} = \mathbf{0} \tag{58}$$

where $\boldsymbol{\lambda}_{i,k}$ and $[\mathbf{T}\hat{\mathbf{S}}_i\mathbf{H}(\mathbf{P}_1\overline{\mathbf{W}}+\mathbf{P}_2\overline{\mathbf{W}}\mathbf{P}_3)]_{k,:}$, respectively, denote the kth component of $\boldsymbol{\lambda}_i$ and the kth row of $\mathbf{T}\hat{\mathbf{S}}_i\mathbf{H}(\mathbf{P}_1\overline{\mathbf{W}} + \mathbf{P}_2\overline{\mathbf{W}}\mathbf{P}_3)$.

The stationarity condition in (58) can be attained by setting the partial derivative of $\mathcal{L}(\overline{\mathbf{W}}, \{\boldsymbol{\lambda}_i\})$ with respect to the primal variable $\overline{\mathbf{W}}$ to zero

$$\sum_{i=1}^{N_s} 2\overline{\mathbf{W}}\left(\mathbf{s}_{:,i}\mathbf{s}_{:,i}^{\mathrm{T}} + \mathbf{P}_3\mathbf{s}_{:,i}\mathbf{s}_{:,i}^{\mathrm{T}}\mathbf{P}_3^{\mathrm{T}}\right) - \mathbf{P}_1^{\mathrm{T}}\mathbf{H}^{\mathrm{T}}\hat{\mathbf{S}}_i^{\mathrm{T}}\mathbf{T}^{\mathrm{T}}\boldsymbol{\lambda}_i\mathbf{s}_{:,i}^{\mathrm{T}} - \mathbf{P}_2^{\mathrm{T}}\mathbf{H}^{\mathrm{T}}\hat{\mathbf{S}}_i^{\mathrm{T}}\mathbf{T}^{\mathrm{T}}\boldsymbol{\lambda}_i\mathbf{s}_{:,i}^{\mathrm{T}}\mathbf{P}_3^{\mathrm{T}} = \mathbf{0}. \tag{59}$$

When $N_s \geq N_r$, the rank of matrix $\sum_{i=1}^{N_s} \mathbf{s}_{:,i}\mathbf{s}_{:,i}^{\mathrm{T}} + \mathbf{P}_3\mathbf{s}_{:,i}\mathbf{s}_{:,i}^{\mathrm{T}}\mathbf{P}_3^{\mathrm{T}}$ is $2N_r$, indicating that it is nonsingular. With this information, the optimal solution to the real-valued PM problem (53) is given by

$$\overline{\mathbf{W}} = \frac{1}{2}\left(\sum_{i=1}^{N_s} \mathbf{P}_1^{\mathrm{T}}\mathbf{H}^{\mathrm{T}}\hat{\mathbf{S}}_i^{\mathrm{T}}\mathbf{T}^{\mathrm{T}}\boldsymbol{\lambda}_i\mathbf{s}_{:,i}^{\mathrm{T}} + \mathbf{P}_2^{\mathrm{T}}\mathbf{H}^{\mathrm{T}}\hat{\mathbf{S}}_i^{\mathrm{T}}\mathbf{T}^{\mathrm{T}}\boldsymbol{\lambda}_i\mathbf{s}_{:,i}^{\mathrm{T}}\mathbf{P}_3^{\mathrm{T}}\right) \times \left(\sum_{i=1}^{N_s} \mathbf{s}_{:,i}\mathbf{s}_{:,i}^{\mathrm{T}} + \mathbf{P}_3\mathbf{s}_{:,i}\mathbf{s}_{:,i}^{\mathrm{T}}\mathbf{P}_3^{\mathrm{T}}\right)^{-1}. \tag{60}$$

The KKT conditions indicate that the primal variable can optimize the Lagrangian function $\mathcal{L}(\overline{\mathbf{W}}, \{\boldsymbol{\lambda}_i\})$ at the zero derivative point. Having obtained the optimal solution in (60), we can substitute it into the Lagrangian function to eliminate the primal variable $\overline{\mathbf{W}}$. This process allows us to obtain the dual function, as given by Proposition 2 below.

Proposition 2: Assuming that $N_s \geq N_r$, the dual function of the problem for the PM slot-invariant IE precoder (53) is given by

$$g(\boldsymbol{\lambda}) \triangleq -\frac{1}{4}\boldsymbol{\lambda}^{\mathrm{T}}\mathbf{U}\boldsymbol{\lambda} + \boldsymbol{\lambda}^{\mathrm{T}}\mathbf{b}. \tag{61}$$

Proof: See Appendix A. ■

As a result, we obtain the dual problem for the PM slot-invariant IE precoder (53) as follows:

$$\min_{\boldsymbol{\lambda}} \ \frac{1}{4}\boldsymbol{\lambda}^{\mathrm{T}}\mathbf{U}\boldsymbol{\lambda} - \mathbf{b}^{\mathrm{T}}\boldsymbol{\lambda} \ \text{s.t.} \ \boldsymbol{\lambda} \succeq \mathbf{0}. \tag{62}$$

Compared with the primal problem in (53), the structure of the dual problem in (62) is much simpler. First, the two problems have different optimization variables. By deriving the dual problem, we reduce the dimension of the optimization variable from $2N_sN_t \times 2N_sN_r$ to $2N_sN_r$. Second, although both problems are linearly constrained quadratic programming problems, the nonnegative constraints in the dual problem are easier to handle compared to the polyhedral constraints in the primal problem. For example, when considering a Euclidean projection problem with nonnegative constraints, we can directly derive its closed-form solution. However, if the problem involves generic polyhedral constraints, a closed-form solution does not exist.

In the scenario where $N_s < N_r$, the rank of matrix $\sum_{i=1}^{N_s} \mathbf{s}_{:,i}\mathbf{s}_{:,i}^{\mathrm{T}} + \mathbf{P}_3\mathbf{s}_{:,i}\mathbf{s}_{:,i}^{\mathrm{T}}\mathbf{P}_3^{\mathrm{T}}$ is $2N_s$ and thus it is singular. A unique Moore–Penrose pseudoinverse can be used to replace the matrix inverse of $\sum_{i=1}^{N_s} \mathbf{s}_{:,i}\mathbf{s}_{:,i}^{\mathrm{T}} + \mathbf{P}_3\mathbf{s}_{:,i}\mathbf{s}_{:,i}^{\mathrm{T}}\mathbf{P}_3^{\mathrm{T}}$ in the above optimal structure and dual problem.

C. SB Slot-Invariant IE Precoder

Following the previous designs for block-level slot-variant and slot-invariant IE precoders, the slot-invariant IE precoder proposed in this section can also be applied to the weighted SB problem. As a result, the complex-valued optimization problem for the weighted SB slot-invariant IE precoder can be represented as

$$\begin{aligned} \max_{\tilde{\mathbf{W}},t} \quad & t \\ \text{s.t.} \quad & \Re\left\{\hat{\mathbf{h}}_k^{\mathrm{T}}\tilde{\mathbf{W}}\tilde{\mathbf{s}}_{:,i}\right\} - \frac{\left|\Im\left\{\hat{\mathbf{h}}_k^{\mathrm{T}}\tilde{\mathbf{W}}\tilde{\mathbf{s}}_{:,i}\right\}\right|}{\tan\frac{\pi}{\mathcal{M}}} \geq t\sqrt{\gamma_{k,i}}\sigma \quad \forall k \quad \forall i \\ & \sum_{i=1}^{N_s}\left\|\tilde{\mathbf{W}}\tilde{\mathbf{s}}_{:,i}\right\|^2 \leq \sum_{i=1}^{N_s} p_i. \end{aligned} \tag{63}$$

The real-valued form of (63) can be written as

$$\begin{aligned} \max_{\overline{\mathbf{W}},t} \quad & t \\ \text{s.t.} \quad & \mathbf{T}\hat{\mathbf{S}}_i\mathbf{H}\left(\mathbf{P}_1\overline{\mathbf{W}} + \mathbf{P}_2\overline{\mathbf{W}}\mathbf{P}_3\right)\mathbf{s}_{:,i} \geq t\mathbf{b}_i \quad \forall i \\ & \sum_{i=1}^{N_s}\left\|\left(\mathbf{P}_1\overline{\mathbf{W}} + \mathbf{P}_2\overline{\mathbf{W}}\mathbf{P}_3\right)\mathbf{s}_{:,i}\right\|^2 \leq \sum_{i=1}^{N_s} p_i. \end{aligned} \tag{64}$$

Similar to Proposition 1, the above block-level transmit power constraint is also active as long as optimality is achieved.

When $\{\sqrt{\gamma_{k,i}}\sigma\}$ equals 1, this problem is equivalent to the optimization problem proposed in [36], referred to as CI-BLP, in which the *symbol-scaling* CI metric was employed to formulate the problem that maximizes the minimum CI effect of an entire transmission block and subject to a block-level power constraint.

D. Optimal Structure for SB Slot-Invariant IE Precoder

For the sake of completeness, we give the optimal solution to the real-valued problem for SB slot-invariant IE precoder below and omit the derivations

$$\overline{\mathbf{W}} = \frac{1}{2\mu}\left(\sum_{i=1}^{N_s} \mathbf{P}_1^{\mathrm{T}}\mathbf{H}^{\mathrm{T}}\hat{\mathbf{S}}_i^{\mathrm{T}}\mathbf{T}^{\mathrm{T}}\boldsymbol{\lambda}_i\mathbf{s}_{:,i}^{\mathrm{T}} + \mathbf{P}_2^{\mathrm{T}}\mathbf{H}^{\mathrm{T}}\hat{\mathbf{S}}_i^{\mathrm{T}}\mathbf{T}^{\mathrm{T}}\boldsymbol{\lambda}_i\mathbf{s}_{:,i}^{\mathrm{T}}\mathbf{P}_3^{\mathrm{T}}\right) \times \left(\sum_{i=1}^{N_s} \mathbf{s}_{:,i}\mathbf{s}_{:,i}^{\mathrm{T}} + \mathbf{P}_3\mathbf{s}_{:,i}\mathbf{s}_{:,i}^{\mathrm{T}}\mathbf{P}_3^{\mathrm{T}}\right)^{-1} \tag{65}$$

where $\mu = (1/2)\sqrt{([\boldsymbol{\lambda}^{\mathrm{T}}\mathbf{U}\boldsymbol{\lambda}]/\sum_{i=1}^{N_s} p_i)}$.

Following a procedure similar to that in Sections III-D and IV-B, the dual problem of (64) can be shown to be

$$\min_{\boldsymbol{\lambda}} \ \boldsymbol{\lambda}^{\mathrm{T}}\mathbf{U}\boldsymbol{\lambda} \ \text{s.t.} \ \boldsymbol{\lambda} \succeq \mathbf{0}, \ \ \mathbf{b}^{\mathrm{T}}\boldsymbol{\lambda} - 1 = 0. \tag{66}$$

E. Duality Between PM and SB Slot-Invariant IE Precoders

In this section, we investigate the properties of the PM and SB slot-invariant IE precoding problems, and extend the explicit duality for block-level slot-variant IE precoding proposed in Section III-E to slot-invariant IE precoding.

Let $\tilde{\mathbf{W}}^{PM}(\{\gamma_{k,i}\})$ and $\sum_{i=1}^{N_s} p_i^{PM}(\{\gamma_{k,i}\}) \triangleq \sum_{i=1}^{N_s} \|\tilde{\mathbf{W}}^{PM}(\{\gamma_{k,i}\})\tilde{\mathbf{s}}_{:,i}\|^2$ denote the optimal solution and objective value of the block-level PM slot-invariant IE precoding problem (47) given $\{\gamma_{k,i}\}$. $\tilde{\mathbf{W}}^{SB}(\{\gamma_{k,i}\}, \sum_{i=1}^{N_s} p_i)$ and $t^{SB}(\{\gamma_{k,i}\}, \sum_{i=1}^{N_s} p_i)$ are the optimal counterparts for the block-level SB slot-invariant IE precoding problem (63) given $\{\gamma_{k,i}\}$ and $\sum_{i=1}^{N_s} p_i$.

Theorem 4 (Duality for Block-Level Slot-Invariant IE Precoding): The block-level PM slot-invariant IE precoder in (47) and SB slot-invariant IE precoder in (63) are dual problems. The explicit duality between them can be expressed as

$$\tilde{\mathbf{W}}^{SB}\left(\{\gamma_{k,i}\}, \sum_{i=1}^{N_s} p_i\right) = \sqrt{\frac{\sum_{i=1}^{N_s} p_i}{\sum_{i=1}^{N_s} p_i^{PM}\left(\{\gamma_{k,i}\}\right)}} \times \tilde{\mathbf{W}}^{PM}\left(\{\gamma_{k,i}\}\right) \quad \forall i \tag{67}$$

$$t^{SB}\left(\{\gamma_{k,i}\}, \sum_{i=1}^{N_s} p_i\right) = \sqrt{\frac{\sum_{i=1}^{N_s} p_i}{\sum_{i=1}^{N_s} p_i^{PM}\left(\{\gamma_{k,i}\}\right)}} \tag{68}$$

and vice versa as

$$\tilde{\mathbf{W}}^{PM}\left(\{\gamma_{k,i}\}\right) = \frac{1}{t^{SB}\left(\{\gamma_{k,i}\}, \sum_{i=1}^{N_s} p_i\right)} \times \tilde{\mathbf{W}}^{SB}\left(\{\gamma_{k,i}\}, \sum_{i=1}^{N_s} p_i\right) \quad \forall i \tag{69}$$

$$\sum_{i=1}^{N_s} p_i^{PM}\left(\{\gamma_{k,i}\}\right) = \frac{\sum_{i=1}^{N_s} p_i}{\left(t^{SB}\left(\{\gamma_{k,i}\}, \sum_{i=1}^{N_s} p_i\right)\right)^2}. \tag{70}$$

Proof: Verbatim to the proof of [38, Th. 1]. ■

In Section III-E, we derived the relationships between the proposed block-level slot-variant IE precoding and conventional symbol-level IE precoding, facilitating the decomposition of the proposed problems. It is worth noting that these relationships cannot be extended to slot-invariant precoding when $N_s > N_r$ due to the precoder structure constraint in (52).

PM slot-invariant precoding can be implemented by solving its Lagrangian dual problem as described in (62), and the solution for SB slot-invariant precoding can be obtained using Theorem 4.

F. Complexity Analysis

We analyze the complexity of the proposed block-level IE precoders in this section, where (62) is selected as an example. The slot-invariant Lagrangian dual problem in (62) can be reformulated as a second-order cone programming (SOCP)

$$\begin{aligned} \min_{\boldsymbol{\lambda},t} \quad & t \\ \text{s.t.} \quad & \frac{1}{4}\boldsymbol{\lambda}^{\mathrm{T}}\mathbf{U}\boldsymbol{\lambda} - \mathbf{b}^{\mathrm{T}}\boldsymbol{\lambda} \geq t \\ & \boldsymbol{\lambda} \succeq \mathbf{0}. \end{aligned} \tag{71}$$

Given an error bound η such that $t \leq t_{opt} + \eta$, where t_{opt} denotes the optimal value of (71), the arithmetic complexity of the η-solution via interior-point methods is given by [41]

$$\mathrm{Compl}(\mathbf{q}, \eta) = O(1)(m+1)^{1/2}n\left(n^2 + m + w\right)\mathrm{Digits}(\mathbf{q}, \eta) \tag{72}$$

where $\mathbf{q}$ and $\mathrm{Digits}(\mathbf{q}, \eta)$, respectively, denote the data vector and the number of accuracy digits in η-solution, as defined in [41], m is the number of constraints, n is the number of optimization variables, and w is the number of rows of the coefficient matrix in the second-order cone constraints. The structure of (71) indicates that

$$m = 2, n = 2N_sN_r + 1, w = 2N_sN_t + 1. \tag{73}$$

V. Linear Precoder for Interference Exploitation

In this section, we present an in-depth investigation of the existence of a linear precoder for IE. Additionally, we demonstrate the intrinsic connections between the block-level precoders proposed in this article and conventional linear precoders. Furthermore, we propose a novel linear precoder under the assumption that the number of symbol slots does not exceed the number of users. Under this assumption, we can equivalently decompose the slot-invariant IE precoding problem into subproblems over each symbol slot.

We also highlight that the linear precoder can be used to estimate the data symbols in a variety of practical multiantenna systems. A notable example is the QR-maximum likelihood detector (QR-MLD), which estimates the data symbols at the receiver side by performing a QR decomposition of the product of the channel matrix and the linear precoder [42], [43]. As a result, a constant precoding matrix used in a transmission block will reduce the detection complexity.

When SLP or BLP is adopted to design the transmit signal, all the $N_r \times N_s$ received signals within one transmission block can be compactly aggregated in one matrix, which can be written as

$$\tilde{\mathbf{Y}} = \tilde{\mathbf{H}}\tilde{\mathbf{W}}\tilde{\mathbf{S}} + \tilde{\mathbf{N}} = \tilde{\mathbf{H}}\tilde{\mathbf{X}} + \tilde{\mathbf{N}} \tag{74}$$

where

$$\tilde{\mathbf{Y}} \triangleq \begin{bmatrix} \tilde{y}_{1,1} & \cdots & \tilde{y}_{1,N_s} \\ \vdots & \ddots & \vdots \\ \tilde{y}_{N_r,1} & \cdots & \tilde{y}_{N_r,N_s} \end{bmatrix} \in \mathbb{C}^{N_r \times N_s} \tag{75a}$$

$$\tilde{\mathbf{H}} \triangleq \begin{bmatrix} \tilde{\mathbf{h}}_1 & \cdots & \tilde{\mathbf{h}}_{N_r} \end{bmatrix} \in \mathbb{C}^{N_r \times N_t} \tag{75b}$$

$$\tilde{\mathbf{S}} \triangleq \begin{bmatrix} \tilde{\mathbf{s}}_{:,1} & \cdots & \tilde{\mathbf{s}}_{:,N_s} \end{bmatrix} \in \mathbb{C}^{N_r \times N_s} \tag{75c}$$

$$\tilde{\mathbf{N}} \triangleq \begin{bmatrix} \tilde{n}_{1,1} & \cdots & \tilde{n}_{1,N_s} \\ \vdots & \ddots & \vdots \\ \tilde{n}_{N_r,1} & \cdots & \tilde{n}_{N_r,N_s} \end{bmatrix} \in \mathbb{C}^{N_r \times N_s} \tag{75d}$$

$$\tilde{\mathbf{X}} \triangleq \begin{bmatrix} \tilde{\mathbf{x}}_1 & \cdots & \tilde{\mathbf{x}}_{N_s} \end{bmatrix} \in \mathbb{C}^{N_t \times N_s}. \tag{75e}$$

When $N_s \leq N_r$, we can represent the optimal transmit signal matrix as a linear transformation of the data symbols

$$\tilde{\mathbf{X}} = \tilde{\mathbf{W}}\tilde{\mathbf{S}} \tag{76}$$

where

$$\tilde{\mathbf{W}} = \tilde{\mathbf{X}}\tilde{\mathbf{S}}^{\dagger}. \tag{77}$$

If $\tilde{\mathbf{S}}$ has full column rank, we have

$$\tilde{\mathbf{S}}^{\dagger} = \left(\tilde{\mathbf{S}}^H\tilde{\mathbf{S}}\right)^{-1}\tilde{\mathbf{S}}^H. \tag{78}$$

On the other hand, if $\tilde{\mathbf{S}}$ is rank-deficient, we can replace $\tilde{\mathbf{S}}^{\dagger}$ by the Moore–Penrose pseudoinverse matrix of $\tilde{\mathbf{S}}$, which can be readily computed using the singular value decomposition of $\tilde{\mathbf{S}}$.

The precoder in (77) can be regarded as a unified linear transformation matrix applied to the data symbol vectors $\{\tilde{\mathbf{s}}_{:,i}\}$ over the N_s symbol slots. In each symbol slot, the precoded signal or transmit signal can be expressed as

$$\tilde{\mathbf{x}}_i = \tilde{\mathbf{W}}\tilde{\mathbf{s}}_{:,i} \quad \forall i. \tag{79}$$

This linear precoder holds as a general solution, regardless of the construction of the transmit signal matrix $\tilde{\mathbf{X}}$. By extending the above linear structure to IE precoding, we establish the following theorem.

Theorem 5: Let $N_s \leq N_r$, then there exists a linear IE precoder given by

$$\tilde{\mathbf{W}} = \tilde{\mathbf{X}}\tilde{\mathbf{S}}^{\dagger} = \left[\tilde{\mathbf{W}}_1\tilde{\mathbf{s}}_{:,1} \cdots \tilde{\mathbf{W}}_{N_s}\tilde{\mathbf{s}}_{:,N_s}\right]\tilde{\mathbf{S}}^{\dagger} \tag{80}$$

which guarantees a constant precoder for each symbol slot within one transmission block.

Accordingly, for symbol-level IE precoding, we can first solve the $N_s \leq N_r$ SLP problems and acquire the N_s optimal symbol-level precoders $\{\tilde{\mathbf{W}}_i\}$ or equivalently the N_s optimal symbol-level transmit signal vectors $\{\tilde{\mathbf{x}}_i\}$, then construct the linear precoder based on Theorem 5. It is important to note that when $N_s > N_r$, (76) is an over-determined system of linear equations, whose solution in (77) does not necessarily exist.

Remark 1: When the number of symbol slots does not exceed the number of users, i.e., $N_s \leq N_r$, the block-level slot-variant IE precoding and slot-invariant IE precoding generate an identical transmit signal in each symbol slot, which means that the matrix structure constraint in (52) is redundant and can be discarded. Based on Sections III and IV, the slot-variant IE precoding can be decomposed into N_s smaller subproblems over N_s symbol slots, whereas the slot-invariant IE precoding cannot due to the extra structural constraint in (52). Therefore, Theorem 5 indicates that under the assumption of $N_s \leq N_r$, we can address the simpler slot-variant IE precoding problem rather than the slot-invariant IE precoding problem to obtain a linear or slot-invariant IE precoder.

VI. Numerical Results

In this section, numerical results based on Monte Carlo simulations are presented to evaluate the proposed block-level slot-variant and slot-invariant IE precoders, as well as the linear precoder for IE. For the SB problem, the weights of the users' SINR are assumed to be $\gamma_{k,i} = \gamma = 1 \quad \forall k \quad \forall i$. In each symbol slot, the SNR is determined as $\text{SNR} = (p_i/\sigma^2) = (1/\sigma^2) \quad \forall i$. The block-level transmit power budget is set to $\sum_{i=1}^{N_s} p_i = N_s$. For the simulations of the PM problem, we assume each user has an identical SINR threshold, i.e., $\gamma_{k,i} = \gamma \quad \forall k \quad \forall i$. The system setting $N_r \times N_t$ is indicated in the legend of each figure. From Section II we know that the proposed slot-variant and slot-invariant precoding are effective for various channel distributions. We first adopt the typical Rayleigh flat fading channel. Unit noise variance is assumed for PM problems, i.e., $\sigma^2 = 1$. The number of random channel realizations is denoted by N_c.

For clarity, we list the abbreviations of the considered algorithms below.

In simulations for SB problems.

1) *RZF:* Linear RZF precoding with block-level power normalization to satisfy the block-level transmit power budget. The RZF precoding matrix over a transmission block is given by

$$\tilde{\mathbf{W}}_{\text{RZF}} = \frac{1}{f_{\text{RZF}}}\tilde{\mathbf{H}}^H\left(\tilde{\mathbf{H}}\tilde{\mathbf{H}}^H + \sigma^2\mathbf{I}\right)^{-1} \tag{81}$$

where f_{RZF} is a power scaling factor defined by

$$f_{\text{RZF}} = \frac{\left\|\tilde{\mathbf{H}}^H\left(\tilde{\mathbf{H}}\tilde{\mathbf{H}}^H + \sigma^2\mathbf{I}\right)^{-1}\tilde{\mathbf{S}}\right\|_F}{\sqrt{\sum_{i=1}^{N_s} p_i}}. \tag{82}$$

2) *BLP:* Traditional block-level SB interference mitigation precoding in [12], which is solved by the fixed-point method.
3) *SLP:* Symbol-level SB IE precoding (36), whose Lagrangian dual problem is solved by the "quadprog" function in MATLAB.
4) *SV-CVX:* Block-level SB slot-variant IE precoding, which is decomposed into N_s SB-SLP subproblems based on Section III-E. The subproblems are solved

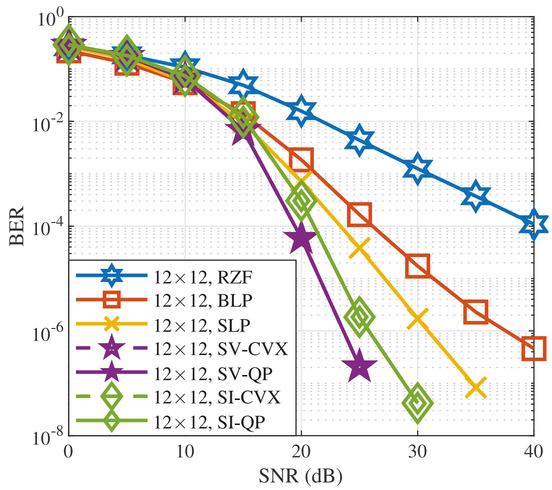

Fig. 2. BER versus SNR, $N_c = 50\,000$, $N_s = 20$, and QPSK.

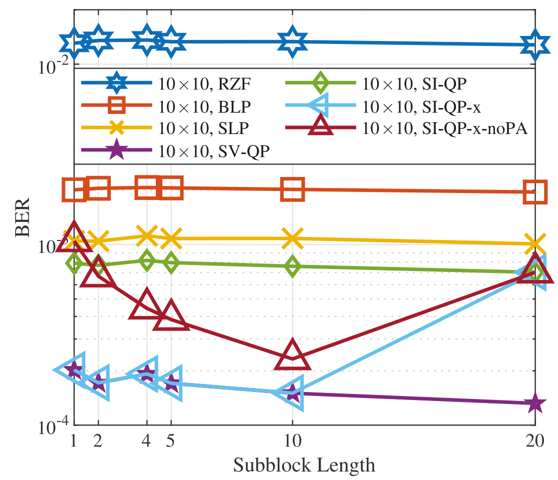

Fig. 3. BER versus subblock length, $N_c = 10\,000$, SNR = 20 dB, and QPSK.

using CVX [44]. Theorem 3 is subsequently applied to compute the optimal solution to the original problem.

5) *SV-QP:* The above SB-SLP subproblems are converted into PM-SLP subproblems, whose Lagrangian dual problems are solved by the quadprog function in MATLAB.
6) *SI-CVX:* Block-level SB slot-invariant IE precoding, which is solved using CVX [44].
7) *SI-QP:* The block-level SB slot-invariant IE precoding problem is converted to its PM counterpart based on Section IV-E. The Lagrangian dual problem of the block-level PM slot-invariant IE precoding problem is solved by the quadprog function in MATLAB.

In simulations for PM problems.

1) *ZF:* Linear ZF precoding with power rescaling to satisfy the SINR thresholds. The ZF precoding matrix over a transmission block is given by

$$\tilde{\mathbf{W}}_{ZF} = \sqrt{\gamma}\sigma \tilde{\mathbf{H}}^H \left(\tilde{\mathbf{H}}\tilde{\mathbf{H}}^H\right)^{-1}. \tag{83}$$

2) *BLP:* Traditional block-level PM interference mitigation precoding in [12], which is solved by the fixed-point method.
3) *SLP:* Symbol-level PM IE precoding (35), whose Lagrangian dual problem is solved by the quadprog function in MATLAB.
4) *SV-CVX:* Block-level PM slot-variant IE precoding, which is decomposed into N_s PM-SLP subproblems based on Section III-E. The subproblems are solved using CVX [44].
5) *SV-QP:* The above subproblems are converted into their Lagrangian dual problems, then solved by the quadprog function in MATLAB.
6) *SI-CVX:* Block-level PM slot-invariant IE precoding, which is solved using CVX [44].
7) *SI-QP:* The above problem is converted into its Lagrangian dual problem, which is solved by the quadprog function in MATLAB.

Fig. 2 compares the BER performance of the considered SB precoding schemes for different SNR. It shows that when the number of symbol slots exceeds the number of users, the proposed SB slot-variant IE precoding has the best BER performance due to its joint optimization without the matrix structure constraint over a transmission block/frame. Moreover, the two proposed optimal structures for slot-variant and slot-invariant precoders achieve the same BER performance as their original optimization problems solved by CVX. This validates the effectiveness of the optimal structures and duality.

To further demonstrate the proposed precoders, we divided each transmission block/frame into several subblocks. We let "SI-QP-x" represent "SI-QP" implemented with a subblock of length "x." Fig. 3 depicts the BER performance as a function of the subframe length. For each subframe in the SI-QP-x approach, we apply the SB slot-invariant IE precoding and the power allocation scheme described in Theorem 3. In comparison, we also include the BER performance of the SI-QP-x method without power allocation, denoted as "SI-QP-x-noPA." Fig. 3 demonstrates that when the subblock length does not exceed the number of users, SI-QP-x exhibits the same BER performance as "SV-QP" due to the presence of an intrinsic linear precoding structure for IE. As the subblock length increases, there is a tradeoff between BER performance and subblock length. Furthermore, this figure illustrates that power allocation within subblocks indeed enhances the BER performance. For SI-QP-x-noPA, a valley point is observed when the subblock length equals the number of users. This can be explained in two ways. First, when the subblock length does not exceed the number of users, the BER performance continues to decrease as the subblock length increases. This occurs because a longer subblock length relaxes the block-level transmit power constraint, enlarging the feasible region and consequently improving performance. Second, when the subblock length exceeds the number of users, the linear precoder proposed in Section V no longer exists, and we must consider the matrix structure constraint. The longer subblock

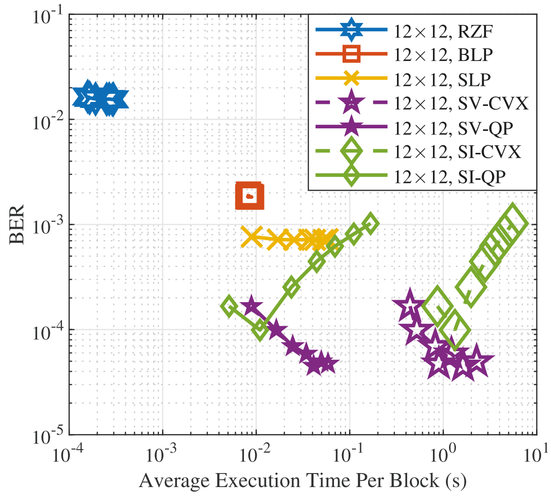

Fig. 4. BER versus average execution time per block, $N_c = 20\,000$, SNR = 20 dB, $N_s = \{6, 12, 18, 24, 30, 36, 42\}$, and QPSK.

length results in a more constrained problem, leading to an increase in BER as the subblock length grows. Therefore, a valley point appears when $N_s = N_r$.

Fig. 4 depicts the BER performance of the considered precoding algorithms in relation to the per block average execution time over a range of block lengths from $N_s = 6$ to $N_s = 42$, demonstrating a direct performance-complexity tradeoff. The block lengths are set to $\{6, 12, 18, 24, 30, 36, 42\}$. In other words, the seven data pairs of BER and execution time are obtained by setting the block length to these seven different values. It is observed that the execution time of the proposed slot-variant and slot-invariant IE precoding schemes generally increases with block length, as it requires more calculations to solve optimization problems with larger dimensions. Furthermore, the results show that the QP solver, aided by the proposed optimal structure and explicit duality, can solve the problems more efficiently than CVX. The slot-variant precoding exhibits the lowest BER due to its separable structure. Its execution time is also shorter than that of the slot-invariant precoding, and comparable to that of conventional SLP.

Fig. 5 presents the BER performance of various SB precoding schemes as a function of the number of users in fully loaded MU-MISO systems. The figure shows that when the number of symbol slots in each transmission block exceeds the number of users, the slot-variant IE precoder demonstrates better BER performance compared to the slot-invariant IE precoder. The performance gap between them is almost proportional to the difference in the number of symbol slots and users. This performance gap disappears when the number of symbol slots equals or is less than the number of users. In scenarios where we divide a transmission block into several subframes, it is observed that when the subframe length does not exceed the number of users, SI-QP-x can achieve the same BER performance as the slot-variant IE precoding, thanks to the power allocation scheme.

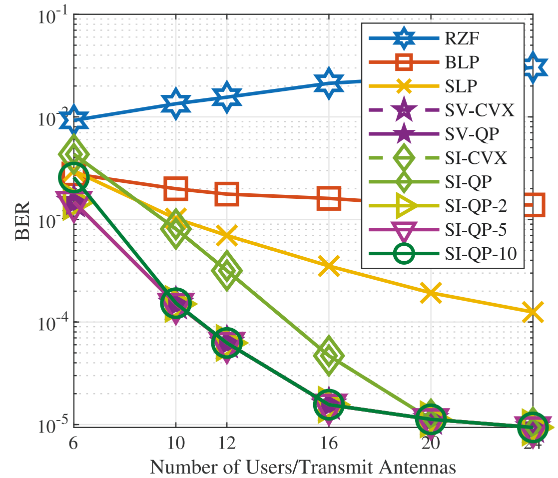

Fig. 5. BER versus number of users/transmit antennas, $N_c = 1000$, $N_s = 20$, SNR = 20 dB, and QPSK.

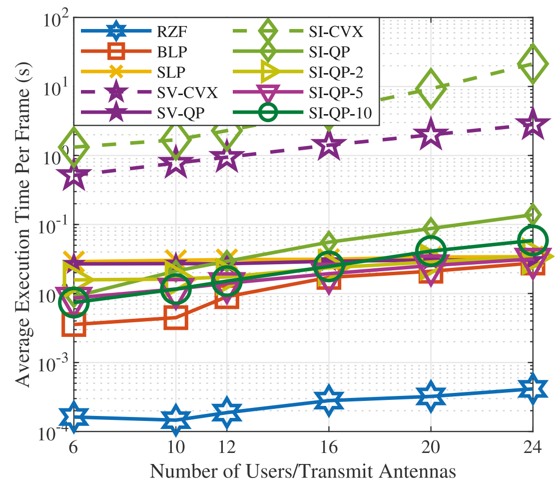

Fig. 6. Average execution time versus number of users/transmit antennas, $N_c = 1000$, $N_s = 20$, SNR = 20 dB, and QPSK.

Fig. 6 illustrates the average execution time per frame of the SB precoding schemes presented in Fig. 5. By employing the proposed optimal structure and explicit duality, the QP approach exhibits superior efficiency compared to the original problem solved by CVX, for both slot-invariant and slot-variant IE precoders. Furthermore, the slot-variant IE precoder requires far less processing time than the slot-invariant IE precoder because of its less-constrained formulation enabling us to decompose the problem into several subproblems with smaller variable sizes, which suggests that slot-variant IE precoder is preferred in the scenario where the number of symbol slots does not exceed the number of users. This validates our idea of the linear precoder for IE in Section V. When dividing a transmission block into several subframes, with each subframe utilizing a constant precoder, the execution time of SI-QP-x is generally shorter than that of SI-QP. This observation can be interpreted as a performance-complexity tradeoff and indicates that by compromising the frame length, we can enhance the efficiency of the slot-invariant IE precoding scheme.

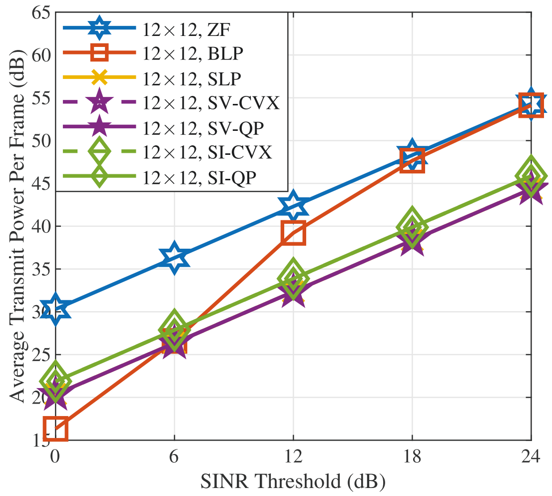

Fig. 7. Average transmit power per frame versus SINR threshold, $N_c = 100$, $N_s = 20$, and QPSK.

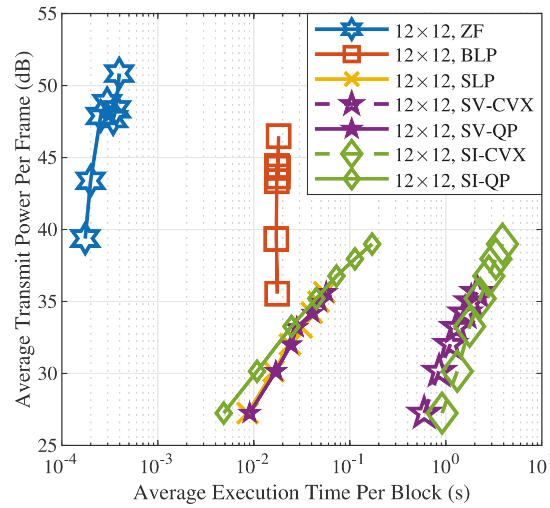

Fig. 9. Average transmit power versus average execution time per block, $N_c = 2000$, $\gamma = 12$ dB, $N_s = \{6, 12, 18, 24, 30, 36, 42\}$, and QPSK.

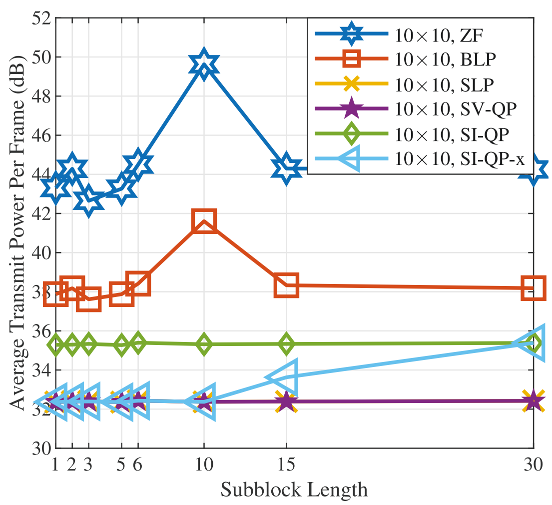

Fig. 8. Average transmit power per frame versus subblock length, $\gamma = 12$ dB, $Nc = 2000$, $N_s = 30$, and QPSK.

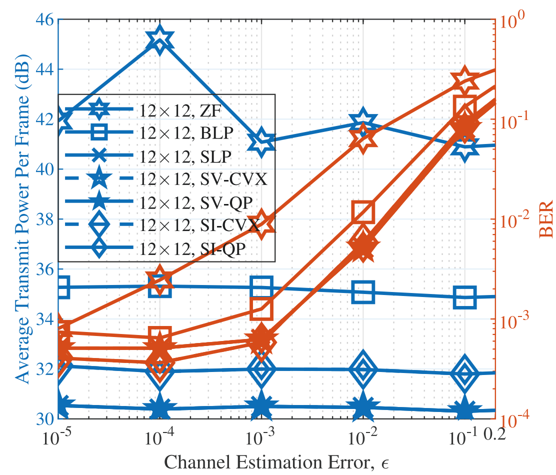

Fig. 10. Average transmit power and BER versus channel estimation error, $N_c = 200$, $\gamma = 10$ dB, $N_s = 20$, and QPSK.

Fig. 7 compares the average block-level transmit power of various precoding schemes amongst different SINR thresholds for PM problems. The transmit power of the QP approach is demonstrated to be consistent with its original formulation solved by CVX, thus highlighting the effectiveness of the proposed optimal structure. It can be seen that when the number of symbol slots is larger than the number of users, PM slot-variant IE precoding always has the lowest block-level transmit power. The power gain comes from the joint optimization without the matrix structure constraint over a transmission block.

Fig. 8 plots the average transmit power per frame as a function of the subblock length. It is observed that when the subblock length does not exceed the number of users, SI-QP-x exhibits the same transmit power performance as SV-QP. However, when the subblock length exceeds the number of users, a larger subblock results in higher transmit power for SI-QP-x.

Fig. 9 demonstrates the performance-complexity tradeoff in terms of average transmit power and average execution time per block. The 7 data pairs for each scheme are obtained by evenly varying the block length from $N_s = 6$ to $N_s = 42$. We observe that the proposed block-level PM slot-variant and slot-invariant IE precoding schemes achieve lower transmit power compared to ZF and traditional BLP, although they generally require more execution time. When the block length is less than 12, the algorithms computed by the QP solver consume less execution time than traditional BLP.

To evaluate the robustness of the proposed slot-variant and slot-invariant precoding to channel estimation error, we assume the BS determines the precoding based on the following imperfect CSI:

$$\bar{\mathbf{H}} = \sqrt{1-\epsilon}\tilde{\mathbf{H}} + \sqrt{\epsilon}\tilde{\mathbf{F}} \tag{84}$$

where $\epsilon \in [0, 1]$, and $\tilde{\mathbf{F}}$ is an error matrix with $\mathcal{CN}(0, 1)$ entries.

Fig. 10 shows the average transmit power and BER performance of the PM problem as a function of the channel estimation error at $\gamma = 10$ dB. It can be seen that ZF and conventional BLP are more sensitive to channel estimation error

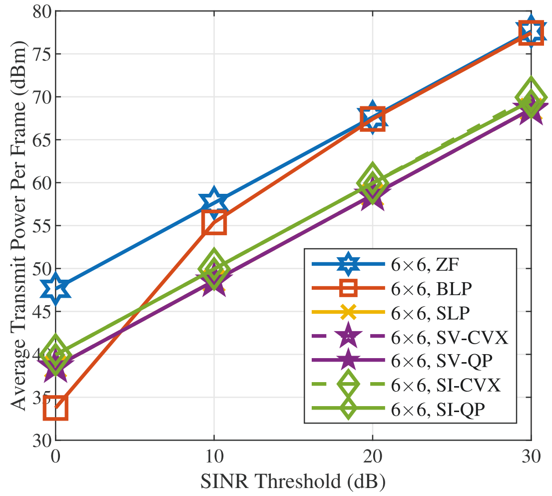

Fig. 11. Average transmit power per frame versus SINR threshold, $N_c = 50$, $N_s = 10$, and QPSK.

than IE precoding. The proposed slot-variant and slot invariant precoders exhibit similar robust performance compared to SLP.

Next we consider a distance-dependent pathloss channel model defined by $L_k(d_k) = C_0(d_k/D_0)^{-\alpha_k}$, where $C_0 = -30$ dB denotes the pathloss at the reference distance $D_0 = 1$ meter (m), while d_k and $\alpha_k = 3.5$ denote the distance and the pathloss exponent from the transmitter to the kth user, respectively. Assume all users are distributed within a circular area of radius 3 m, where the distance between the center of the circle and the transmitter is 53 m. In this case the noise variance is set to $\sigma^2 = -70$ dBm. The channel vector between the transmitter and the kth user is given by

$$\tilde{\mathbf{h}}_k = \sqrt{L_k}\left(\sqrt{\frac{K_F}{1+K_F}}\tilde{\mathbf{h}}_k^{\mathrm{LoS}} + \sqrt{\frac{1}{1+K_F}}\tilde{\mathbf{h}}_k^{\mathrm{NLoS}}\right) \tag{85}$$

where $K_F = 3$ dB denotes the Rician factor, $\tilde{\mathbf{h}}_k^{\mathrm{LoS}}$ and $\tilde{\mathbf{h}}_k^{\mathrm{NLoS}} \sim \mathcal{CN}(\mathbf{0}, \mathbf{I})$ denote the Line-of-Sight (LoS) and the small-scale Rayleigh fading Non Line-of-Sight (NLoS) components, respectively.

Fig. 11 illustrates the performance of the PM solution under the above distance-dependent channel model. We observe that the performance is similar to that in Fig. 7, and again the proposed slot-variant and slot-invariant precoders outperform the other benchmark approaches.

VII. Conclusion

In this article, we have presented block-level slot-variant and slot-invariant IE precoding. Both PM and weighted SB problems have been investigated, leveraging explicit duality. A linear precoder for IE has been further proposed, which can provide uncompromised SLP performance gain. Numerical results have been conducted to validate the effectiveness of the proposed slot-variant and slot-invariant IE precoding. Future works could involve devising practical numerical algorithms for the derived dual problems.

Appendix A
Proof for Proposition 2

For notational simplicity, define $\boldsymbol{\Sigma} \triangleq \sum_{i=1}^{N_s} \mathbf{s}_{:,i}\mathbf{s}_{:,i}^{\mathrm{T}} + \mathbf{P}_3\mathbf{s}_{:,i}\mathbf{s}_{:,i}^{\mathrm{T}}\mathbf{P}_3^{\mathrm{T}}$. Substituting the optimal solution structure in (60) into $\sum_{i=1}^{N_s} \mathbf{s}_{:,i}^{\mathrm{T}}\overline{\mathbf{W}}^{\mathrm{T}}\overline{\mathbf{W}}\mathbf{s}_{:,i}$ and $\sum_{i=1}^{N_s} \mathbf{s}_{:,i}^{\mathrm{T}}\mathbf{P}_3^{\mathrm{T}}\overline{\mathbf{W}}^{\mathrm{T}}\overline{\mathbf{W}}\mathbf{P}_3\mathbf{s}_{:,i}$, we have the following two equations:

$$\begin{aligned}
&\sum_{i=1}^{N_s} \mathbf{s}_{:,i}^{\mathrm{T}}\overline{\mathbf{W}}^{\mathrm{T}}\overline{\mathbf{W}}\mathbf{s}_{:,i}\\
&\quad= \frac{1}{4}\sum_{i=1}^{N_s}\sum_{j=1}^{N_s}\sum_{k=1}^{N_s}\left(\mathbf{s}_{:,k}^{\mathrm{T}}\boldsymbol{\Sigma}^{-1}\mathbf{s}_{:,i}\mathbf{s}_{:,i}^{\mathrm{T}}\boldsymbol{\Sigma}^{-1}\mathbf{s}_{:,j}\right)\\
&\qquad\times \boldsymbol{\lambda}_j^{\mathrm{T}}\mathbf{T}\hat{\mathbf{S}}_j\mathbf{H}\mathbf{P}_1\mathbf{P}_1^{\mathrm{T}}\mathbf{H}^{\mathrm{T}}\hat{\mathbf{S}}_k^{\mathrm{T}}\mathbf{T}^{\mathrm{T}}\boldsymbol{\lambda}_k\\
&\qquad+ \frac{1}{4}\sum_{i=1}^{N_s}\sum_{j=1}^{N_s}\sum_{k=1}^{N_s}\left(\mathbf{s}_{:,k}^{\mathrm{T}}\mathbf{P}_3^{\mathrm{T}}\boldsymbol{\Sigma}^{-1}\mathbf{s}_{:,i}\mathbf{s}_{:,i}^{\mathrm{T}}\boldsymbol{\Sigma}^{-1}\mathbf{s}_{:,j}\right)\\
&\qquad\times \boldsymbol{\lambda}_j^{\mathrm{T}}\mathbf{T}\hat{\mathbf{S}}_j\mathbf{H}\mathbf{P}_1\mathbf{P}_2^{\mathrm{T}}\mathbf{H}^{\mathrm{T}}\hat{\mathbf{S}}_k^{\mathrm{T}}\mathbf{T}^{\mathrm{T}}\boldsymbol{\lambda}_k\\
&\qquad+ \frac{1}{4}\sum_{i=1}^{N_s}\sum_{j=1}^{N_s}\sum_{k=1}^{N_s}\left(\mathbf{s}_{:,k}^{\mathrm{T}}\boldsymbol{\Sigma}^{-1}\mathbf{s}_{:,i}\mathbf{s}_{:,i}^{\mathrm{T}}\boldsymbol{\Sigma}^{-1}\mathbf{P}_3\mathbf{s}_{:,j}\right)\\
&\qquad\times \boldsymbol{\lambda}_j^{\mathrm{T}}\mathbf{T}\hat{\mathbf{S}}_j\mathbf{H}\mathbf{P}_2\mathbf{P}_1^{\mathrm{T}}\mathbf{H}^{\mathrm{T}}\hat{\mathbf{S}}_k^{\mathrm{T}}\mathbf{T}^{\mathrm{T}}\boldsymbol{\lambda}_k\\
&\qquad+ \frac{1}{4}\sum_{i=1}^{N_s}\sum_{j=1}^{N_s}\sum_{k=1}^{N_s}\left(\mathbf{s}_{:,k}^{\mathrm{T}}\mathbf{P}_3^{\mathrm{T}}\boldsymbol{\Sigma}^{-1}\mathbf{s}_{:,i}\mathbf{s}_{:,i}^{\mathrm{T}}\boldsymbol{\Sigma}^{-1}\mathbf{P}_3\mathbf{s}_{:,j}\right)\\
&\qquad\times \boldsymbol{\lambda}_j^{\mathrm{T}}\mathbf{T}\hat{\mathbf{S}}_j\mathbf{H}\mathbf{P}_2\mathbf{P}_2^{\mathrm{T}}\mathbf{H}^{\mathrm{T}}\hat{\mathbf{S}}_k^{\mathrm{T}}\mathbf{T}^{\mathrm{T}}\boldsymbol{\lambda}_k
\end{aligned} \tag{86}$$

$$\begin{aligned}
&\sum_{i=1}^{N_s} \mathbf{s}_{:,i}^{\mathrm{T}}\mathbf{P}_3^{\mathrm{T}}\overline{\mathbf{W}}^{\mathrm{T}}\overline{\mathbf{W}}\mathbf{P}_3\mathbf{s}_{:,i}\\
&\quad= \frac{1}{4}\sum_{i=1}^{N_s}\sum_{j=1}^{N_s}\sum_{k=1}^{N_s}\left(\mathbf{s}_{:,k}^{\mathrm{T}}\boldsymbol{\Sigma}^{-1}\mathbf{P}_3\mathbf{s}_{:,i}\mathbf{s}_{:,i}^{\mathrm{T}}\mathbf{P}_3^{\mathrm{T}}\boldsymbol{\Sigma}^{-1}\mathbf{s}_{:,j}\right)\\
&\qquad\times \boldsymbol{\lambda}_j^{\mathrm{T}}\mathbf{T}\hat{\mathbf{S}}_j\mathbf{H}\mathbf{P}_1\mathbf{P}_1^{\mathrm{T}}\mathbf{H}^{\mathrm{T}}\hat{\mathbf{S}}_k^{\mathrm{T}}\mathbf{T}^{\mathrm{T}}\boldsymbol{\lambda}_k\\
&\quad+ \frac{1}{4}\sum_{i=1}^{N_s}\sum_{j=1}^{N_s}\sum_{k=1}^{N_s}\left(\mathbf{s}_{:,k}^{\mathrm{T}}\mathbf{P}_3^{\mathrm{T}}\boldsymbol{\Sigma}^{-1}\mathbf{P}_3\mathbf{s}_{:,i}\mathbf{s}_{:,i}^{\mathrm{T}}\mathbf{P}_3^{\mathrm{T}}\boldsymbol{\Sigma}^{-1}\mathbf{s}_{:,j}\right)\\
&\qquad\times \boldsymbol{\lambda}_j^{\mathrm{T}}\mathbf{T}\hat{\mathbf{S}}_j\mathbf{H}\mathbf{P}_1\mathbf{P}_2^{\mathrm{T}}\mathbf{H}^{\mathrm{T}}\hat{\mathbf{S}}_k^{\mathrm{T}}\mathbf{T}^{\mathrm{T}}\boldsymbol{\lambda}_k\\
&\quad+ \frac{1}{4}\sum_{i=1}^{N_s}\sum_{j=1}^{N_s}\sum_{k=1}^{N_s}\left(\mathbf{s}_{:,k}^{\mathrm{T}}\boldsymbol{\Sigma}^{-1}\mathbf{P}_3\mathbf{s}_{:,i}\mathbf{s}_{:,i}^{\mathrm{T}}\mathbf{P}_3^{\mathrm{T}}\boldsymbol{\Sigma}^{-1}\mathbf{P}_3\mathbf{s}_{:,j}\right)\\
&\qquad\times \boldsymbol{\lambda}_j^{\mathrm{T}}\mathbf{T}\hat{\mathbf{S}}_j\mathbf{H}\mathbf{P}_2\mathbf{P}_1^{\mathrm{T}}\mathbf{H}^{\mathrm{T}}\hat{\mathbf{S}}_k^{\mathrm{T}}\mathbf{T}^{\mathrm{T}}\boldsymbol{\lambda}_k\\
&\quad+ \frac{1}{4}\sum_{i=1}^{N_s}\sum_{j=1}^{N_s}\sum_{k=1}^{N_s}\left(\mathbf{s}_{:,k}^{\mathrm{T}}\mathbf{P}_3^{\mathrm{T}}\boldsymbol{\Sigma}^{-1}\mathbf{P}_3\mathbf{s}_{:,i}\mathbf{s}_{:,i}^{\mathrm{T}}\mathbf{P}_3^{\mathrm{T}}\boldsymbol{\Sigma}^{-1}\mathbf{P}_3\mathbf{s}_{:,j}\right)\\
&\qquad\times \boldsymbol{\lambda}_j^{\mathrm{T}}\mathbf{T}\hat{\mathbf{S}}_j\mathbf{H}\mathbf{P}_2\mathbf{P}_2^{\mathrm{T}}\mathbf{H}^{\mathrm{T}}\hat{\mathbf{S}}_k^{\mathrm{T}}\mathbf{T}^{\mathrm{T}}\boldsymbol{\lambda}_k.
\end{aligned} \tag{87}$$

To simplify the above expressions, we can rearrange components and utilize the definition of $\boldsymbol{\Sigma}$, resulting in

$$\begin{aligned}
&\sum_{i=1}^{N_s} \mathbf{s}_{:,i}^{\mathrm{T}}\overline{\mathbf{W}}^{\mathrm{T}}\overline{\mathbf{W}}\mathbf{s}_{:,i} + \sum_{i=1}^{N_s} \mathbf{s}_{:,i}^{\mathrm{T}}\mathbf{P}_3^{\mathrm{T}}\overline{\mathbf{W}}^{\mathrm{T}}\overline{\mathbf{W}}\mathbf{P}_3\mathbf{s}_{:,i}\\
&\quad= \frac{1}{4}\sum_{j=1}^{N_s}\sum_{k=1}^{N_s}\left(\mathbf{s}_{:,k}^{\mathrm{T}}\boldsymbol{\Sigma}^{-1}\mathbf{s}_{:,j}\right)\boldsymbol{\lambda}_j^{\mathrm{T}}\mathbf{T}\hat{\mathbf{S}}_j\mathbf{H}\mathbf{P}_1\mathbf{P}_1^{\mathrm{T}}\mathbf{H}^{\mathrm{T}}\hat{\mathbf{S}}_k^{\mathrm{T}}\mathbf{T}^{\mathrm{T}}\boldsymbol{\lambda}_k
\end{aligned}$$

$$+\frac{1}{4}\sum_{j=1}^{N_s}\sum_{k=1}^{N_s}\left(\mathbf{s}_{:,k}^{\mathrm{T}}\mathbf{P}_3^{\mathrm{T}}\boldsymbol{\Sigma}^{-1}\mathbf{s}_{:,j}\right)\boldsymbol{\lambda}_j^{\mathrm{T}}\mathbf{T}\hat{\mathbf{S}}_j\mathbf{H}\mathbf{P}_1\mathbf{P}_2^{\mathrm{T}}\mathbf{H}^{\mathrm{T}}\hat{\mathbf{S}}_k^{\mathrm{T}}\mathbf{T}^{\mathrm{T}}\boldsymbol{\lambda}_k$$
$$+\frac{1}{4}\sum_{j=1}^{N_s}\sum_{k=1}^{N_s}\left(\mathbf{s}_{:,k}^{\mathrm{T}}\boldsymbol{\Sigma}^{-1}\mathbf{P}_3\mathbf{s}_{:,j}\right)\boldsymbol{\lambda}_j^{\mathrm{T}}\mathbf{T}\hat{\mathbf{S}}_j\mathbf{H}\mathbf{P}_2\mathbf{P}_1^{\mathrm{T}}\mathbf{H}^{\mathrm{T}}\hat{\mathbf{S}}_k^{\mathrm{T}}\mathbf{T}^{\mathrm{T}}\boldsymbol{\lambda}_k$$
$$+\frac{1}{4}\sum_{j=1}^{N_s}\sum_{k=1}^{N_s}\left(\mathbf{s}_{:,k}^{\mathrm{T}}\mathbf{P}_3^{\mathrm{T}}\boldsymbol{\Sigma}^{-1}\mathbf{P}_3\mathbf{s}_{:,j}\right)\boldsymbol{\lambda}_j^{\mathrm{T}}\mathbf{T}\hat{\mathbf{S}}_j\mathbf{H}\mathbf{P}_2\mathbf{P}_2^{\mathrm{T}}\mathbf{H}^{\mathrm{T}}\hat{\mathbf{S}}_k^{\mathrm{T}}\mathbf{T}^{\mathrm{T}}\boldsymbol{\lambda}_k. \tag{88}$$

Subsequently, we use the optimal solution structure to rewrite the remaining terms of the Lagrangian, yielding

$$\begin{aligned}
&\sum_{i=1}^{N_s}\boldsymbol{\lambda}_i^{\mathrm{T}}\mathbf{T}\hat{\mathbf{S}}_i\mathbf{H}\mathbf{P}_1\overline{\mathbf{W}}\mathbf{s}_{:,i}+\boldsymbol{\lambda}_i^{\mathrm{T}}\mathbf{T}\hat{\mathbf{S}}_i\mathbf{H}\mathbf{P}_2\overline{\mathbf{W}}\mathbf{P}_3\mathbf{s}_{:,i}\\
&=\frac{1}{2}\sum_{i=1}^{N_s}\sum_{j=1}^{N_s}\left(\mathbf{s}_{:,j}^{\mathrm{T}}\boldsymbol{\Sigma}^{-1}\mathbf{s}_{:,i}\right)\boldsymbol{\lambda}_i^{\mathrm{T}}\mathbf{T}\hat{\mathbf{S}}_i\mathbf{H}\mathbf{P}_1\mathbf{P}_1^{\mathrm{T}}\mathbf{H}^{\mathrm{T}}\hat{\mathbf{S}}_j^{\mathrm{T}}\mathbf{T}^{\mathrm{T}}\boldsymbol{\lambda}_j\\
&+\frac{1}{2}\sum_{i=1}^{N_s}\sum_{j=1}^{N_s}\left(\mathbf{s}_{:,j}^{\mathrm{T}}\mathbf{P}_3^{\mathrm{T}}\boldsymbol{\Sigma}^{-1}\mathbf{s}_{:,i}\right)\boldsymbol{\lambda}_i^{\mathrm{T}}\mathbf{T}\hat{\mathbf{S}}_i\mathbf{H}\mathbf{P}_1\mathbf{P}_2^{\mathrm{T}}\mathbf{H}^{\mathrm{T}}\hat{\mathbf{S}}_j^{\mathrm{T}}\mathbf{T}^{\mathrm{T}}\boldsymbol{\lambda}_j\\
&+\frac{1}{2}\sum_{i=1}^{N_s}\sum_{j=1}^{N_s}\left(\mathbf{s}_{:,j}^{\mathrm{T}}\boldsymbol{\Sigma}^{-1}\mathbf{P}_3\mathbf{s}_{:,i}\right)\boldsymbol{\lambda}_i^{\mathrm{T}}\mathbf{T}\hat{\mathbf{S}}_i\mathbf{H}\mathbf{P}_2\mathbf{P}_1^{\mathrm{T}}\mathbf{H}^{\mathrm{T}}\hat{\mathbf{S}}_j^{\mathrm{T}}\mathbf{T}^{\mathrm{T}}\boldsymbol{\lambda}_j\\
&+\frac{1}{2}\sum_{i=1}^{N_s}\sum_{j=1}^{N_s}\left(\mathbf{s}_{:,j}^{\mathrm{T}}\mathbf{P}_3^{\mathrm{T}}\boldsymbol{\Sigma}^{-1}\mathbf{P}_3\mathbf{s}_{:,i}\right)\boldsymbol{\lambda}_i^{\mathrm{T}}\mathbf{T}\hat{\mathbf{S}}_i\mathbf{H}\mathbf{P}_2\mathbf{P}_2^{\mathrm{T}}\mathbf{H}^{\mathrm{T}}\hat{\mathbf{S}}_j^{\mathrm{T}}\mathbf{T}^{\mathrm{T}}\boldsymbol{\lambda}_j.
\end{aligned}\tag{89}$$

After the above manipulations, the dual function is given by

$$\begin{aligned}
&g(\{\boldsymbol{\lambda}_i\})\triangleq\min_{\overline{\mathbf{W}}}\mathcal{L}\left(\overline{\mathbf{W}},\{\boldsymbol{\lambda}_i\}\right)\\
&=-\frac{1}{4}\sum_{i=1}^{N_s}\sum_{j=1}^{N_s}\left(\mathbf{s}_{:,j}^{\mathrm{T}}\boldsymbol{\Sigma}^{-1}\mathbf{s}_{:,i}\right)\boldsymbol{\lambda}_i^{\mathrm{T}}\mathbf{T}\hat{\mathbf{S}}_i\mathbf{H}\mathbf{P}_1\mathbf{P}_1^{\mathrm{T}}\mathbf{H}^{\mathrm{T}}\hat{\mathbf{S}}_j^{\mathrm{T}}\mathbf{T}^{\mathrm{T}}\boldsymbol{\lambda}_j\\
&\quad-\frac{1}{4}\sum_{i=1}^{N_s}\sum_{j=1}^{N_s}\left(\mathbf{s}_{:,j}^{\mathrm{T}}\mathbf{P}_3^{\mathrm{T}}\boldsymbol{\Sigma}^{-1}\mathbf{s}_{:,i}\right)\boldsymbol{\lambda}_i^{\mathrm{T}}\mathbf{T}\hat{\mathbf{S}}_i\mathbf{H}\mathbf{P}_1\mathbf{P}_2^{\mathrm{T}}\mathbf{H}^{\mathrm{T}}\hat{\mathbf{S}}_j^{\mathrm{T}}\mathbf{T}^{\mathrm{T}}\boldsymbol{\lambda}_j\\
&\quad-\frac{1}{4}\sum_{i=1}^{N_s}\sum_{j=1}^{N_s}\left(\mathbf{s}_{:,j}^{\mathrm{T}}\boldsymbol{\Sigma}^{-1}\mathbf{P}_3\mathbf{s}_{:,i}\right)\boldsymbol{\lambda}_i^{\mathrm{T}}\mathbf{T}\hat{\mathbf{S}}_i\mathbf{H}\mathbf{P}_2\mathbf{P}_1^{\mathrm{T}}\mathbf{H}^{\mathrm{T}}\hat{\mathbf{S}}_j^{\mathrm{T}}\mathbf{T}^{\mathrm{T}}\boldsymbol{\lambda}_j\\
&\quad-\frac{1}{4}\sum_{i=1}^{N_s}\sum_{j=1}^{N_s}\left(\mathbf{s}_{:,j}^{\mathrm{T}}\mathbf{P}_3^{\mathrm{T}}\boldsymbol{\Sigma}^{-1}\mathbf{P}_3\mathbf{s}_{:,i}\right)\\
&\quad\times\boldsymbol{\lambda}_i^{\mathrm{T}}\mathbf{T}\hat{\mathbf{S}}_i\mathbf{H}\mathbf{P}_2\mathbf{P}_2^{\mathrm{T}}\mathbf{H}^{\mathrm{T}}\hat{\mathbf{S}}_j^{\mathrm{T}}\mathbf{T}^{\mathrm{T}}\boldsymbol{\lambda}_j+\sum_{i=1}^{N_s}\boldsymbol{\lambda}_i^{\mathrm{T}}\mathbf{b}_i\\
&=-\frac{1}{4}\boldsymbol{\lambda}^{\mathrm{T}}\mathbf{U}\boldsymbol{\lambda}+\boldsymbol{\lambda}^{\mathrm{T}}\mathbf{b}
\end{aligned}\tag{90}$$

where

$$\boldsymbol{\lambda}\triangleq\left[\boldsymbol{\lambda}_1^{\mathrm{T}},\ldots,\boldsymbol{\lambda}_{N_s}^{\mathrm{T}}\right]^{\mathrm{T}}\in\mathbb{R}^{2N_sN_r} \tag{91a}$$
$$\mathbf{U}\triangleq\begin{bmatrix}\mathbf{U}_{1,1}&\cdots&\mathbf{U}_{1,N_s}\\ \vdots&\ddots&\vdots\\ \mathbf{U}_{N_s,1}&\cdots&\mathbf{U}_{N_s,N_s}\end{bmatrix}\in\mathbb{R}^{2N_sN_r\times 2N_sN_r} \tag{91b}$$
$$\begin{aligned}
\mathbf{U}_{i,j}\triangleq&\left(\mathbf{s}_{:,j}^{\mathrm{T}}\boldsymbol{\Sigma}^{-1}\mathbf{s}_{:,i}\right)\mathbf{T}\hat{\mathbf{S}}_i\mathbf{H}\mathbf{P}_1\mathbf{P}_1^{\mathrm{T}}\mathbf{H}^{\mathrm{T}}\hat{\mathbf{S}}_j^{\mathrm{T}}\mathbf{T}^{\mathrm{T}}\\
&+\left(\mathbf{s}_{:,j}^{\mathrm{T}}\mathbf{P}_3^{\mathrm{T}}\boldsymbol{\Sigma}^{-1}\mathbf{s}_{:,i}\right)\mathbf{T}\hat{\mathbf{S}}_i\mathbf{H}\mathbf{P}_1\mathbf{P}_2^{\mathrm{T}}\mathbf{H}^{\mathrm{T}}\hat{\mathbf{S}}_j^{\mathrm{T}}\mathbf{T}^{\mathrm{T}}\\
&+\left(\mathbf{s}_{:,j}^{\mathrm{T}}\boldsymbol{\Sigma}^{-1}\mathbf{P}_3\mathbf{s}_{:,i}\right)\mathbf{T}\hat{\mathbf{S}}_i\mathbf{H}\mathbf{P}_2\mathbf{P}_1^{\mathrm{T}}\mathbf{H}^{\mathrm{T}}\hat{\mathbf{S}}_j^{\mathrm{T}}\mathbf{T}^{\mathrm{T}}\\
&+\left(\mathbf{s}_{:,j}^{\mathrm{T}}\mathbf{P}_3^{\mathrm{T}}\boldsymbol{\Sigma}^{-1}\mathbf{P}_3\mathbf{s}_{:,i}\right)\mathbf{T}\hat{\mathbf{S}}_i\mathbf{H}\mathbf{P}_2\mathbf{P}_2^{\mathrm{T}}\mathbf{H}^{\mathrm{T}}\hat{\mathbf{S}}_j^{\mathrm{T}}\mathbf{T}^{\mathrm{T}}.
\end{aligned}\tag{91c}$$

References

[1] E. G. Larsson, O. Edfors, F. Tufvesson, and T. L. Marzetta, "Massive MIMO for next generation wireless systems," *IEEE Commun. Mag.*, vol. 52, no. 2, pp. 186–195, Feb. 2014.

[2] L. Lu, G. Y. Li, A. L. Swindlehurst, A. Ashikhmin, and R. Zhang, "An overview of massive MIMO: Benefits and challenges," *IEEE J. Sel. Topics Signal Process.*, vol. 8, no. 5, pp. 742–758, Oct. 2014.

[3] L. Zheng and D. N. C. Tse, "Diversity and multiplexing: A fundamental tradeoff in multiple-antenna channels," *IEEE Trans. Inf. Theory*, vol. 49, no. 5, pp. 1073–1096, May 2003.

[4] N. D. Sidiropoulos, T. N. Davidson, and Z.-Q. Luo, "Transmit beamforming for physical-layer multicasting," *IEEE Trans. Signal Process.*, vol. 54, no. 6, pp. 2239–2251, Jun. 2006.

[5] C. Windpassinger, R. F. H. Fischer, T. Vencel, and J. B. Huber, "Precoding in multiantenna and multiuser communications," *IEEE Trans. Wireless Commun.*, vol. 3, no. 4, pp. 1305–1316, Jul. 2004.

[6] G. Caire and S. Shamai, "On the achievable throughput of a multiantenna gaussian broadcast channel," *IEEE Trans. Inf. Theory*, vol. 49, no. 7, pp. 1691–1706, Jul. 2003.

[7] C. B. Peel, B. M. Hochwald, and A. L. Swindlehurst, "A vector-perturbation technique for near-capacity multiantenna multiuser communication-Part I: Channel inversion and regularization," *IEEE Trans. Commun.*, vol. 53, no. 1, pp. 195–202, Jan. 2005.

[8] M. Costa, "Writing on dirty paper (Corresp.)," *IEEE Trans. Inf. Theory*, vol. 29, no. 3, pp. 439–441, May 1983.

[9] B. M. Hochwald, C. B. Peel, and A. L. Swindlehurst, "A vector-perturbation technique for near-capacity multiantenna multiuser communication-Part II: Perturbation," *IEEE Trans. Commun.*, vol. 53, no. 3, pp. 537–544, Mar. 2005.

[10] M. Bengtsson and B. Ottersten, "Optimal downlink beamforming using semidefinite optimization," in *Proc. 37th Annu. Allerton Conf. Commun., Control Comput.*, 1999, pp. 987–996.

[11] M. Bengtsson and B. Ottersten, "Optimum and suboptimum transmit beamforming," in *Handbook of Antennas in Wireless Communications*. Boca Raton, FL, USA: CRC Press, 2002, p. 18.

[12] A. Wiesel, Y. C. Eldar, and S. Shamai, "Linear precoding via conic optimization for fixed MIMO receivers," *IEEE Trans. Signal Process.*, vol. 54, no. 1, pp. 161–176, Jan. 2006.

[13] E. Karipidis, N. D. Sidiropoulos, and Z.-Q. Luo, "Quality of service and max-min fair transmit beamforming to multiple cochannel multicast groups," *IEEE Trans. Signal Process.*, vol. 56, no. 3, pp. 1268–1279, Mar. 2008.

[14] C. Masouros and E. Alsusa, "A novel transmitter-based selective-precoding technique for DS/CDMA systems," *IEEE Signal Process. Lett.*, vol. 14, no. 9, pp. 637–640, Sep. 2007.

[15] C. Masouros and E. Alsusa, "Dynamic linear precoding for the exploitation of known interference in MIMO broadcast systems," *IEEE Trans. Wireless Commun.*, vol. 8, no. 3, pp. 1396–1404, Mar. 2009.

[16] C. Masouros, "Correlation rotation linear precoding for MIMO broadcast communications," *IEEE Trans. Signal Process.*, vol. 59, no. 1, pp. 252–262, Jan. 2011.

[17] M. Alodeh, S. Chatzinotas, and B. Ottersten, "Constructive multiuser interference in symbol level precoding for the MISO downlink channel," *IEEE Trans. Signal Process.*, vol. 63, no. 9, pp. 2239–2252, May 2015.

[18] C. Masouros and G. Zheng, "Exploiting known interference as green signal power for downlink beamforming optimization," *IEEE Trans. Signal Process.*, vol. 63, no. 14, pp. 3628–3640, Jul. 2015.

[19] A. Li et al., "A tutorial on interference exploitation via symbol-level precoding: Overview, state-of-the-art and future directions," *IEEE Commun. Surveys Tuts.*, vol. 22, no. 2, pp. 796–839, 2nd Quart., 2020.

[20] M. Alodeh, S. Chatzinotas, and B. Ottersten, "Energy-efficient symbol-level precoding in multiuser MISO based on relaxed detection region," *IEEE Trans. Wireless Commun.*, vol. 15, no. 5, pp. 3755–3767, May 2016.

[21] M. Alodeh, S. Chatzinotas, and B. Ottersten, "Symbol-level multiuser MISO precoding for multi-level adaptive modulation," *IEEE Trans. Wireless Commun.*, vol. 16, no. 8, pp. 5511–5524, Aug. 2017.

[22] A. Haqiqatnejad, F. Kayhan, and B. Ottersten, "Symbol-level precoding design based on distance preserving constructive interference regions," *IEEE Trans. Signal Process.*, vol. 66, no. 22, pp. 5817–5832, Nov. 2018.

[23] S. Domouchtsidis, C. G. Tsinos, S. Chatzinotas, and B. Ottersten, "Symbol-level precoding for low complexity transmitter architectures in large-scale antenna array systems," *IEEE Trans. Wireless Commun.*, vol. 18, no. 2, pp. 852–863, Feb. 2019.

[24] D. Spano, M. Alodeh, S. Chatzinotas, and B. Ottersten, "Symbol-level precoding for the nonlinear multiuser MISO downlink channel," *IEEE Trans. Signal Process.*, vol. 66, no. 5, pp. 1331–1345, Mar. 2018.

[25] M. Alodeh et al., "Symbol-level and multicast precoding for multiuser multiantenna downlink: A state-of-the-art, classification, and challenges," *IEEE Commun. Surveys Tuts.*, vol. 20, no. 3, pp. 1733–1757, 3rd Quart., 2018.

[26] A. Li, L. Song, B. Vucetic, and Y. Li, "Interference exploitation precoding for reconfigurable intelligent surface aided multi-user communications with direct links," *IEEE Commun. Lett.*, vol. 9, no. 11, pp. 1937–1941, Nov. 2020.

[27] R. Liu, M. Li, Q. Liu, A. L. Swindlehurst, and Q. Wu, "Intelligent reflecting surface based passive information transmission: A symbol-level precoding approach," *IEEE Trans. Veh. Technol.*, vol. 70, no. 7, pp. 6735–6749, Jul. 2021.

[28] R. Liu, M. Li, Q. Liu, and A. L. Swindlehurst, "Joint symbol-level precoding and reflecting designs for IRS-enhanced MU-MISO systems," *IEEE Trans. Wireless Commun.*, vol. 20, no. 2, pp. 798–811, Feb. 2021.

[29] L. Wu, B. Wang, Z. Cheng, M. R. B. Shankar, and B. Ottersten, "Joint symbol-level precoding and sub-block-level RIS design for dual-function radar-communications," in *Proc. IEEE Int. Conf. Acoust. Speech Signal Process. (ICASSP)*, 2023, pp. 1–5.

[30] A. Li, F. Liu, C. Masouros, Y. Li, and B. Vucetic, "Interference exploitation 1-bit massive MIMO Precoding: A partial branch-and-bound solution with near-optimal performance," *IEEE Trans. Wireless Commun.*, vol. 19, no. 5, pp. 3474–3489, May 2020.

[31] A. Li, C. Masouros, A. L. Swindlehurst, and W. Yu, "1-bit massive MIMO transmission: Embracing interference with symbol-level precoding," *IEEE Commun. Mag.*, vol. 59, no. 5, pp. 121–127, May 2021.

[32] Z. Wu, B. Jiang, Y.-F. Liu, M. Shao, and Y.-H. Dai, "Efficient CI-based one-bit precoding for multiuser downlink massive MIMO systems with PSK modulation," *IEEE Trans. Wireless Commun.*, vol. 23, no. 5, pp. 4861–4875, May 2024.

[33] F. Liu, C. Masouros, A. Li, T. Ratnarajah, and J. Zhou, "MIMO radar and cellular coexistence: A power-efficient approach enabled by interference exploitation," *IEEE Trans. Signal Process.*, vol. 66, no. 14, pp. 3681–3695, Jul. 2018.

[34] R. Liu, M. Li, Q. Liu, and A. L. Swindlehurst, "Dual-functional radar-communication waveform design: A symbol-level precoding approach," *IEEE J. Sel. Topics Signal Process.*, vol. 15, no. 6, pp. 1316–1331, Nov. 2021.

[35] Y. Chen, F. Liu, Z. Liao, and F. Dong, "Symbol-level precoding for MIMO ISAC transmission based on interference exploitation," *IEEE Commun. Lett.*, vol. 28, no. 2, pp. 283–287, Feb. 2024.

[36] A. Li, C. Shen, X. Liao, C. Masouros, and A. L. Swindlehurst, "Practical interference exploitation precoding without symbol-by-symbol optimization: A block-level approach," *IEEE Trans. Wireless Commun.*, vol. 22, no. 6, pp. 3982–3996, Jun. 2023.

[37] Y. Liu, M. Shao, W.-K. Ma, and Q. Li, "Symbol-level precoding through the lens of zero forcing and vector perturbation," *IEEE Trans. Signal Process.*, vol. 70, pp. 1687–1703, Feb. 2022.

[38] J. Yang, A. Li, X. Liao, and C. Masouros, "Speeding-up symbol-level precoding using separable and dual Optimizations," *IEEE Trans. Commun.*, vol. 71, no. 12, pp. 7056–7071, Dec. 2023.

[39] Y. Wang, H. Hou, W. Wang, X. Yi, and S. Jin, "Soft demodulator for symbol-level precoding in coded multiuser MISO systems," *IEEE Trans. Wireless Commun.*, early access, Jul. 3, 2024, doi: 10.1109/TWC.2024.3419258.

[40] A. Kalantari et al., "*M*-QAM Precoder design for MIMO directional modulation transceivers," 2018, *arXiv:1702.06878*.

[41] A. Ben-Tal and A. Nemirovski, *Lectures on Modern Convex Optimization: Analysis Algorithms and Engineering Applications*. Philadelphia, PA, USA: SIAM, 2001.

[42] M. O. Damen, H. El Gamal, and G. Caire, "On maximum-likelihood detection and the search for the closest lattice point," *IEEE Trans. Inf. Theory*, vol. 49, no. 10, pp. 2389–2402, Oct. 2003.

[43] S. Yang and L. Hanzo, "Fifty years of MIMO detection: The road to large-scale MIMOs," *IEEE Commun. Surveys Tuts.*, vol. 17, no. 4, pp. 1941–1988, 4th Quart., 2015.

[44] M. Grant and S. Boyd. "CVX: MATLAB software for disciplined convex programming, version 2.1." Mar. 2014. [Online]. Available: http://cvxr.com/cvx

Junwen Yang (Graduate Student Member, IEEE) received the B.S. degree in electronic information engineering and the M.S. degree in electronic and communication engineering from Central China Normal University, Wuhan, China, in 2017 and 2019, respectively. He is currently pursuing the Ph.D. degree with the School of Information and Communications Engineering, Xi'an Jiaotong University, Xi'an, China.

His current research interests mainly focus on wireless communications, signal processing, optimization, and symbol-level precoding.

Ang Li (Senior Member, IEEE) received the Ph.D. degree from the Communications and Information Systems Research Group, Department of Electrical and Electronic Engineering, University College London, London, U.K., in April 2018.

He was a Postdoctoral Research Associate with the School of Electrical and Information Engineering, The University of Sydney, Sydney, Sydney, NSW, Australia, from May 2018 to February 2020. He was with Xi'an Jiaotong University, Xi'an, China, in March 2020, where he is currently a Professor with the School of Information and Communications Engineering, Faculty of Electronic and Information Engineering. His main research interests lie in the physical-layer techniques in wireless communications, including MIMO/massive MIMO, interference exploitation, symbol-level precoding, and reconfigurable MIMO.

Dr. Li currently serves as an Associate Editor for IEEE COMMUNICATIONS LETTERS, IEEE OPEN JOURNAL OF SIGNAL PROCESSING, and EURASIP JOURNAL ON WIRELESS COMMUNICATIONS AND NETWORKING. He has been an Exemplary Reviewer for IEEE COMMUNICATIONS LETTERS, IEEE TRANSACTIONS ON COMMUNICATIONS, and IEEE WIRELESS COMMUNICATIONS LETTERS. He has served as the Co-Chair for the IEEE ICASSP 2020 Special Session on "Hardware-Efficient Large-Scale Antenna Arrays: The Stage for Symbol-Level Precoding," and has organized a Tutorial in IEEE ICC 2021 on "Interference Exploitation through Symbol Level Precoding: Energy Efficient Transmission for 6G and Beyond."

Xuewen Liao (Member, IEEE) received the B.S. and Ph.D. degrees in information and communications engineering from Xi'an Jiaotong University, Xi'an, China, in 2002 and 2008, respectively.

From 2008 to 2012, he was an Assistant Professor with Xi'an Jiaotong University. From 2016 to 2017, he was a Visiting Scholar with the Department of Electrical and Computer Engineering, The University of British Columbia, Vancouver, BC, Canada. He is currently a Professor with the School of Information and Communications Engineering, Xi'an Jiaotong University. His research interests include wireless energy transfer, green communications, relay communications, and indoor positioning.

Christos Masouros (Fellow, IEEE) received the Diploma degree in electrical and computer engineering from the University of Patras, Patras, Greece, in 2004, and the M.Sc. degree by research and the Ph.D. degree in electrical and electronic engineering from The University of Manchester, Manchester, U.K., in 2006 and 2009, respectively.

In 2008, he was a Research Intern with Philips Research Laboratory, Surrey, U.K., working on the LTE Standards. From 2009 to 2010, he was a Research Associate with The University of Manchester and from 2010 to 2012 a Research Fellow with Queen's University Belfast, Belfast, U.K. In 2012, he was a Lecturer with the University College London, London, U.K. He has held a Royal Academy of Engineering Research Fellowship from 2011 to 2016. Since 2019, he has been a Full Professor of Signal Processing and Wireless Communications with the Information and Communication Engineering Research Group, Department Electrical and Electronic Engineering, and affiliated with the Institute for Communications and Connected Systems, University College London. From 2018 to 2022, he was the Project Coordinator of the 4.2m EU H2020 ITN Project PAINLESS, involving 12 EU partner universities and industries, toward energy-autonomous networks. From 2024–2028, he will be the Scientific Coordinator of the 2.7m EU H2020 DN Project ISLANDS, involving 19 EU Partner Universities and Industries, toward next generation vehicular networks. His research interests lie in the field of wireless communications and signal processing with particular focus on green communications, large scale antenna systems, integrated sensing and communications, interference mitigation techniques for MIMO and multicarrier communications.

Dr. Masouros was the recipient of the 2023 IEEE ComSoc Stephen O. Rice Prize, co-recipient of the 2021 IEEE SPS Young Author Best Paper Award, and the recipient of the Best Paper Awards in the IEEE GlobeCom 2015 and IEEE WCNC 2019 Conferences. He is an IEEE ComSoc Distinguished Lecturer from 2024 to 2025, has been recognised as an Exemplary Editor for the IEEE COMMUNICATIONS LETTERS and as an Exemplary Reviewer for the IEEE TRANSACTIONS ON COMMUNICATIONS. He is an Editor for IEEE TRANSACTIONS ON WIRELESS COMMUNICATIONS, the IEEE OPEN JOURNAL OF SIGNAL PROCESSING, and Editor-at-Large for IEEE OPEN JOURNAL OF THE COMMUNICATIONS SOCIETY. He has been an Editor for IEEE TRANSACTIONS ON COMMUNICATIONS and IEEE COMMUNICATIONS LETTERS, and a Guest Editor for a number of IEEE JOURNAL ON SELECTED TOPICS IN SIGNAL PROCESSING and IEEE JOURNAL ON SELECTED AREAS IN COMMUNICATIONS issues. He is a Founding Member and the Vice-Chair of the IEEE Emerging Technology Initiative on Integrated Sensing and Communications, the Vice Chair of the IEEE Wireless Communications Technical Committee Special Interest Group on ISAC, and the Chair of the IEEE Green Communications and Computing Technical Committee, the Special Interest Group on Green ISAC. He is a member of the IEEE Standards Association Working Group on ISAC Performance Metrics and a Founding Member of the ETSI ISG on ISAC. He is the TPC Chair for the IEEE ICC 2024 Selected Areas in Communications Track on ISAC, and the Chair of the "Integrated Imaging and Communications" stream in IEEE CISA 2024. He is a Fellow of the Asia–Pacific Artificial Intelligence Association.

A. Lee Swindlehurst (Fellow, IEEE) received the B.S. and M.S. degrees in electrical engineering from Brigham Young University (BYU), Provo, UT, USA, in 1985 and 1986, respectively, and the Ph.D. degree in electrical engineering from Stanford University, Stanford, CA, USA, in 1991.

He was with the Department of Electrical and Computer Engineering, BYU from 1990 to 2007, where he served as a Department Chair from 2003 to 2006. From 1996 to 1997, he held a joint appointment as a Visiting Scholar with Uppsala University, Uppsala, Sweden, and the Royal Institute of Technology in Sweden. From 2006 to 2007, he was on leave working as a Vice President of Research for ArrayComm LLC, San Jose, CA, USA. Since 2007, he has been with the Electrical Engineering and Computer Science Department, University of California Irvine, Irvine, CA, USA, where he is a Distinguished Professor and currently serving as a Department Chair. His research focuses on array signal processing for radar, wireless communications, and biomedical applications.

Dr. Swindlehurst received the 2000 IEEE W. R. G. Baker Prize Paper Award, the 2006 IEEE Communications Society Stephen O. Rice Prize in the Field of Communication Theory, the 2006, 2010, and 2021 IEEE Signal Processing Society's Best Paper Awards, the 2017 IEEE Signal Processing Society Donald G. Fink Overview Paper Award, a Best Paper award at the 2020 and 2024 IEEE International Conferences on Communications, the 2022 Claude Shannon-Harry Nyquist Technical Achievement Award from the IEEE Signal Processing Society, and the 2024 Fred W. Ellersick Prize from the IEEE Communications Society. He was also a Hans Fischer Senior Fellow in the Institute for Advanced Studies at the Technical University of Munich, from 2014 to 2017, and in 2016, he was elected as a Foreign Member of the Royal Swedish Academy of Engineering Sciences.